Published in final edited form as:
Magn Reson Imaging Clin N Am. 2014 August ; 22(3): 373–395. doi:10.1016/j.mric.2014.04.009.

DIFFUSION-WEIGHTED IMAGING OF THE LIVER: TECHNIQUES AND APPLICATIONS

Sara Lewis, MD[1], **Hadrien Dyvorne, PhD**[2], **Yong Cui, MD**[2], and **Bachir Taouli, MD**[1,2]

[1]Department of Radiology, Icahn School of Medicine at Mount Sinai, One Gustave Levy Place, Box 1234, New York, NY 10029, USA

[2]Translational and Molecular Imaging Institute, Icahn School of Medicine at Mount Sinai, One Gustave Levy Place, Box 1234, New York, NY 10029, USA

SYNOPSIS

Diffusion weighted MRI (DWI) is a technique that assesses the cellularity, tortuosity of the extracellular/extravascular space and cell membrane density based upon differences in water proton mobility in tissues. The strength of the diffusion weighting is reflected by the b-value. DWI using several b-values enables quantification of the apparent diffusion coefficient (ADC). DWI is increasingly employed in liver imaging for multiple reasons: it can add useful qualitative and quantitative information to conventional imaging sequences, it is acquired relatively quickly, it is easily incorporated into existing clinical protocols, and it is a non-contrast technique. DWI is useful for focal liver lesion detection and characterization, for the assessment of post-treatment tumor response and for evaluation of diffuse liver disease. ADC quantification can be used to characterize lesions as cystic/necrotic or solid and for predicting tumor response to therapy. Advanced diffusion methods such as IVIM (intravoxel incoherent motion) may have potential for detection, staging and evaluation of the progression of liver fibrosis and for liver lesion characterization. The lack of standardization of DWI technique including choice of b-values and sequence parameters has somewhat limited its widespread adoption.

Keywords

Diffusion; liver MRI; apparent diffusion coefficient; liver lesion detection; liver lesion characterization; IVIM; cirrhosis; echo planar imaging

INTRODUCTION

Diffusion weighted imaging (DWI) is a magnetic resonance imaging (MRI) technique that reports on the physical process of microscopic thermal motion of water molecules in biologic tissues[1,2]. The differences in the mobility of water protons create image contrast,

Corresponding author: Bachir Taouli, MD, bachir.taouli@mountsinai.org.

which is influenced by the interaction of water molecules with cellular membranes, macromolecules, degree of cellular density and the size of the extracellular extravascular space[3]. DWI is increasingly being employed in liver MRI given recent technologic advances and improvements in image quality, including the introduction of echo planar imaging (EPI), parallel imaging, multichannel coils and high amplitude gradients.

Accurate lesion detection and characterization is essential for treatment planning for patients with primary or secondary liver tumors, especially in selecting patients who may undergo liver resection, loco-regional or systemic therapies[4,5]. DWI can be employed for focal liver lesion detection and characterization, for the assessment of tumor response, and for evaluation of diffuse liver disease[3]. This sequence is easily incorporated into routine clinical protocols, especially given that DWI is a non-contrast technique and may be performed either before or after contrast administration. DWI can be acquired rapidly within a breath hold, and it provides both qualitative and quantitative information as an adjunct to conventional sequences. Quantification of apparent diffusion coefficient (ADC) has enabled differentiation of solid cellular lesions from cystic or necrotic lesions[6]. ADC quantification has also demonstrated promising results for predicting tumor response to therapy[7,8]. The purpose of this chapter is to review the basic principles of DWI, discuss protocol optimization, summarize the performance of DWI compared to conventional sequences, discuss the role of DWI in evaluation of treatment response and examine the potential role of DWI in the assessment of liver fibrosis.

DWI TECHNIQUE

1. Concepts

1.1. Principles of molecular diffusion—Diffusion describes random molecular motion occurring in tissues as a result of thermally activated translations of atoms and molecules. The resulting motion can be described as a stochastic process, with a Gaussian probability distribution given as:

$$P(r,t) \sim e^{-\frac{r^2}{4Dt}} \quad \text{Eq. 1}$$

where *D* is the diffusion coefficient and *r* is the distance traveled by the diffusing molecule during time *t. D* depends on the species undergoing diffusion and on the medium in which diffusion occurs. For water self-diffusion at 37° C, $D = 3.0\ mm^2/s$ [9]. Larger molecules tend to undergo slower diffusion resulting in lower *D*, as is also the case of diffusion in fluids of higher viscosity. The Gaussian distribution in Eq. 1 describes free diffusion of molecules in an infinite medium. An important variation of this concept is restricted diffusion where molecular motion is restrained within hard boundaries. Restricted diffusion, which is common in tissues, generally leads to lower *D* and non-Gaussian distributions.

1.2. DWI physics—Nuclear magnetic resonance offers an novel way to measure diffusion, via the application of magnetic field gradients. If such gradients are deployed in pulses of opposed polarity (using a gradient or spin echo sequence), moving spins undergo dephasing while static spins show a null phase at the echo time. By considering the effect of a

stochastic diffusion process on the magnetic signal, one can derive the signal attenuation resulting from the application of pulsed gradients in a spin echo experiment[10]:

$$S = S_0 e^{-bD}$$

with S_0 the signal in the absence of gradient and b a function of the applied gradient:

$$b = (\gamma G \delta)^2 \left(\Delta - \frac{\delta}{3} \right)$$

with γ the spin gyromagnetic ratio, G and δ the gradient strength and length, and Δ the time separating the gradient pair. The factor b, called b-value, determines the strength of the diffusion weighing. The diffusion gradients can be inserted in an imaging experiment as a preparation module, in order to provide additional contrast to the MRI signal and to estimate molecular diffusion in different organs and tissues.

1.3. Quantification of diffusion properties in tissues—In its simplest form, the diffusion experiment involves acquiring two sets of images, one at low or zero b-value, another at high b-value, to derive a voxel-wise diffusion coefficient. Since multiple tissues and compartments may be present in a single voxel, the derived coefficient is referred to as an ADC that reflects a sum of exponential decays rather than a single, pure diffusion constant. In addition to the ADC, which assumes monoexponential decay of diffusion signal, there are models that account for the more complex properties of tissues:

- Flowing blood contributes to diffusion signal and leads to measureable effects on the diffusion decay. The intravoxel incoherent motion (IVIM) approach[11] integrates these effects in a biexponential model where a faster decaying exponential, reflecting perfusion effects at low b-values, can be separated from slower exponential decay reflecting true water diffusion. This approach is especially appropriate in highly perfused organs such as the liver[12–18].
- Because of restricted diffusion in tissues, the Gaussian model of Eq. 1 is not valid anymore, and diffusion weighting has a less trivial form. A successful approach has been diffusion kurtosis imaging (DKI) that evaluates restricted diffusion by analyzing the non-Gaussian diffusion distribution, using an additional constant derived from acquisitions at higher b-value[19]. Recently, DKI has been investigated in liver explant studies, where results have been correlated with hepatocellular carcinoma (HCC) tumor cellularity[20].
- Biological tissues can be anisotropic, and therefore so can diffusion decay. The ADC measured using different diffusion gradient directions may differ in an anisotropic sample, therefore diffusion tensor imaging[21] (DTI) has been proposed in order to extract direction-specific information using at least 6 different diffusion gradient directions. In the liver, acquisition protocols typically involve acquiring the diffusion trace, which is an average of all 3 principal diffusion directions. DTI

has been investigated in abdominal organs[22–25], but there is limited data on anisotropic properties in the liver [26–28].

1.4. Quality control—There are sources of variability for diffusion quantification across different platforms or centers. First, hardware variations exist between different platforms, leading to different estimates for ADC. Sasaki et al[29] reported up to 9% variability in brain ADC in a multicenter study in 12 healthy subjects. Chenevert et al[30] measured the ADC of a temperature-controlled ice-water sample in several platforms and reported 5% variability across 3 vendors at 1.5T and 3T. Another source for variability is the choice of b-values used to derive the ADC. Previous studies in liver DWI have used a b-value range of 0–1000 s/mm^2. Because of confounding effects of perfusion, computing the ADC using a lower range of b-values (e.g. 0–400) may lead to higher values than using an extended range of b-values (e.g. 0–1000), and to different accuracy of the technique for disease detection[31]. According to Xing et al[32], the ADC can be reliably estimated using 2 b-values chosen outside of the perfusion range, with magnitude such that $b_{high}-b_{low}\sim 1.1/D$. In order to measure perfusion effects using the IVIM model, more b-values are needed and the b-values distributions must be appropriately chosen to sample the fast pseudo-diffusion ($b<100$) and slower true diffusion ($100<b<1000$) decays[33,34].

1.5. Reproducibility and repeatability—Reproducibility and repeatability are important concepts for quantitative diffusion evaluation, particularly for longitudinal and multicentre studies. In the liver, Braithwaite et al[35] reported mean coefficient of variation (CV=standard deviation divided by mean) of 14%. In hepatic tumors[36], similar results were reported for short term reproducibility (95% limits of agreement: 30%), and ADC reproducibility was found to depend on lesion location (lower reproducibility in the left lobe) and size (lower reproducibility in smaller lesions). The reproducibility of liver IVIM was also reported[13,14,17], showing higher reproducibility for D and ADC (CV <20%), compared to perfusion parameters PF (or *f*) and D* (or Dt) (CV >20%). IVIM reproducibility was further investigated in lesions in a recent study showing lower reproducibility of IVIM parameters in liver metastases[13] and HCC[37] compared to liver parenchyma. These findings may be due to higher variability of physiological processes in HCC, or to limitations of DWI for measurement of finite size lesions (lesions DWI signal is more sensitive to motion artifacts and to limited resolution).

2. Diffusion acquisition

2.1. Imaging strategy—The most widely used strategy for DWI is echo planar imaging (EPI), which allows acquisition of a full slice in a single shot. A typical protocol involves using fat-saturated single shot diffusion weighted EPI played in an interleaved multislice fashion to allow volume coverage. However, the EPI readout is also subject to ghosting and susceptibility artifacts[38]. Some alternative techniques to EPI include:

- Segmented EPI[39], which is performed by distributing the EPI acquisition over repeated cycles. This way, susceptibility artifacts are reduced by decreasing the EPI readout length. Compared to single shot EPI, segmented EPI is more sensitive to motion occurring between consecutive shots, leading to signal inconsistency and artifacts.

- Turbo spin echo[40] (TSE) and steady state free precession[41] (SSFP), which may offer reduced B_0 and susceptibility artifacts compared to EPI readouts. However this usually leads to increased echo trains, and to higher power deposition of the radiofrequency pulse train.
- PROPELLER[42], a modified segmented EPI technique where successive segments are acquired in a radial fashion. Compared to segmented EPI, PROPELLER may be more immune to motion artifacts, with options for robust motion correction[43].

2.2. Control of physiologic motion—Physiologic motion is inherent to any liver imaging protocol, with breathing and cardiac motion resulting in subject and acquisition-dependent imaging artifacts. Single shot EPI is robust to motion because its acquisition time is faster than physiological processes. However, in a typical DWI acquisition with multiple b-values and signal averaging, residual fluctuations exist between successively acquired EPI images. Either breath hold (BH), free breathing (FB) or respiratory triggering (RT) technique may be employed. BH results in the shortest image acquisition time, with a limitation in the number of b-values that can be used. FB protocols typically result in blurred images. RT acquisition (using navigator echoes or bellows) may improve DWI data quality[14,36,44,45], at the cost of increased imaging time. Cardiac motion artifacts usually appear in the left liver lobe as signal loss at high b-value, as a result of strong dephasing of coherently moving spins under the influence of diffusion gradients. This can be overcome by performing DWI acquisitions at diastole using an ECG or pulse trigger[46], but this approach results in significantly increased scan time. Another promising approach to mitigate signal loss due to cardiac motion is to use motion-compensated diffusion gradients[47,48] to cancel the dephasing of coherently moving tissues while maintaining diffusion-weighting.

2.3. Parallel imaging—Using multiple receiver radiofrequency coils, k-space acquisition can be accelerated by skipping lines and reconstructing the image using well established algorithms[49–51]. Applied to single shot EPI, parallel imaging allows for shorter EPI train, hence lower susceptibility artifacts and achievable higher resolution[52]. In order to avoid residual artifacts and severe signal loss, acceleration factors are typically limited to 3, depending on the number of coil elements. Another more recent application of parallel imaging is multiband imaging that allows for simultaneous excitation and acquisition of multiple slices[53,54]. Multiband imaging leads to increased slice coverage compared to regular DWI acquisition, with minimal signal degradation.

2.4. Effect of magnetic field strength: 1.5 vs. 3T—Because of the strong signal attenuation imposed by diffusion gradients, DWI suffers from low signal levels, as quantified by the signal to noise ratio (SNR). Low SNR, especially at high b-values, can be overcome by signal averaging or by increased static magnetic field. In this regard, a magnetic field strength of 3T might result in up to 2-fold SNR increase compared to 1.5T (4-fold reduction in signal averaging). However, Rozenkrantz et al[55] reported worse image quality for abdominal DWI at 3T when compared to 1.5T. This study was using a first generation 3T system. Physical limitations at 3T may explain the moderate advantages of 3T DWI. First, higher EPI distortions may arise from stronger B_0 and susceptibility variations.

Second, the radiofrequency wavelength at 3T, of the same order as the human body, results in inhomogeneity of the excitation field B_1. This in turn may lead to large signal variations across the liver and ghosting artifacts due to incomplete fat saturation. In addition to image quality degradation, previous reports have shown significant differences in ADC of abdominal organs at 1.5T and 3T[56]. Fig. 1 illustrates DWI artifacts at 3T compared to 1.5T.

LIVER APPLICATIONS

1. Lesion Detection

Detection of malignant liver lesions is predicated on the belief that tumors have increased cellularity compared to background liver parenchyma and, consequentially, higher signal intensity on DWI. DWI is increasingly employed in oncologic imaging for detection of liver metastases, HCC and cholangiocarcinoma, the application of which will be discussed in detail below. Low b-value diffusion images using SS EPI (i.e. b <100) are most valuable for lesion detection given the suppression of vascular flow, producing “black blood” images, resulting in improved conspicuity for lesions located near vessels[57,58]. The suppression of intrahepatic vascular flow also avoids confusing a small lesion with a vessel on the T2WI sequence[57]. Compared to high b-value images (i.e. b1000), low b-value images have relatively higher contrast-to-noise and signal-to-noise ratios[58–61]. Low b-value images are also less affected by signal loss due to cardiac motion and geometric distortions induced by eddy currents[62]. Prior work has compared DWI lesion detection rates with conventional sequences, including T2 weighted images and post-contrast T1 weighted imaging (CE T1WI) using extracellular gadolinium based contrast agents (GBCAs), liver specific GBCAs and non-GBCAs liver specific agents, as discussed below. Studies comparing DWI to superparamagnetic iron oxide (SPIO) or mangafodipir trisodium (MnDPDP) will not be discussed in this review as these agents are either no longer available or not widely used.

1.1. Liver metastases—The accurate diagnosis of liver metastases is critical for treatment planning and for identifying patients suitable for liver resection, locoregional therapy or systemic chemotherapy[63–65]. MRI provides valuable and accurate information regarding lesion size, segmental location and distribution of liver metastases[4,66]. DWI has outperformed T2WI in several studies for liver lesion detection (including metastases), with DWI detection rates as high as 71–87.7% versus 55.6–70.1% for T2WI[57,67–71]. A current challenge remains the ability to detect small lesions, especially metastases <2 cm in size. In a prospective study of 129 lesions including 40 metastases, Coenegrachts et al demonstrated that 100% of metastases < 1 cm (40/40) were detected on low b-value DWI (b=20). Similarly, Parikh et al showed excellent metastatic lesion detection rate of 78.5% (57/72) for DWI compared to 45.8% (33/72) for T2WI for lesions 1–2 cm in size. In a retrospective series of 118 hepatic metastases, Bruegel et al reported DWI detection rate of 88–91% versus 45–62% for T2WI, a result that was also impressive for small lesions <1 cm, with DWI detection rate of 85% versus 26–44% for T2WI sequences[68]. The superior detection rates of optimized RT DWI may be explained by improved image quality compared to T2WI with a reduction in eddy current induced artifacts and image blurring[6]. Furthermore, diffusion images also have improved background fat saturation, suppression of intrahepatic vascular flow and liver to lesion contrast compared to T2WI[58,67].

Routine liver MRI protocols typically include post-contrast T1WI for the detection of liver metastases. Both extracellular and combined extracellular-hepatocyte specific GBCAs such as gadoxetic acid (Primovist/Eovist, Bayer Healthcare) are widely used. DWI is not significantly affected by gadoxetic acid injection, and in order to minimize table time, DWI may be obtained between the dynamic and hepatobiliary (HBP) phases[72]. Results comparing DWI with dynamic CE T1WI and/or HBP for the detection of liver metastases have been mixed with most studies evaluating hypovascular metastases. Overall, DWI performs reasonably well compared to CE-MRI, with equivocal or slightly lower detection rates reported in most series. A recent meta-analysis by Wu et al examined the overall diagnostic value of DWI in detecting liver metastases and to compared its performance with CE-MRI[62]. The authors examined 11 studies (9 retrospective, 2 prospective) with 537 patients using either a variety of GBCAs or liver specific agents for comparison with DWI. These results show no major difference in the performance of DWI compared to either extra-cellular GBCAs or combined GBCAs[68,70,73–81]. DWI used in combination with CE-MRI or HBP imaging demonstrates higher sensitivity compared to DWI alone, with pooled sensitivities across multiple studies of 97% for the combined set versus 86% for DWI alone[62]. The sensitivity of DWI was statistically equivalent when compared to CE-MRI in several recent studies (66.3–84.4% vs. 76.0–79.7%, respectively)[70,75,79]. Subgroup analysis in several of these studies also showed that DWI is highly accurate in detecting small lesions. For example, Lowenthal et al demonstrated 92% sensitivity of DWI for detecting lesions <1 cm[80]. In a recent retrospective study of 144 pathologically proven metastases, the authors noted that assessment of DWI was very important in identifying small lesions, which may be missed or misinterpreted as peripheral vessels or imaging artifacts on HBP[82]. Interestingly, per-lesion analysis in the study by Hardie et al[75] revealed a trend towards improved DWI detection rate for the less experienced observer for both lesions <1 cm and >1 cm, without reaching statistical significance. This finding was thought to be due to the simplicity of interpretation of DWI (Fig. 2, 3). Recent publications have evaluated DWI for detection of hypervascular liver metastases. DWI outperformed CE-MRI in a retrospective series of 41 patients with 162 hypervascular neuroendocrine liver metastases, with sensitivities of 71.6%–71.0% versus 47.5%–48.1% (P= 0.001)[69]. Further work is necessary to compare of the role of DWI for hypervascular and hypovascular liver metastases.

Summary: DWI is highly sensitive for detection of liver metastases, especially for small lesions < 2 cm. Combined DWI and CE T1WI yields the best performance for lesion detection compared to each sequence alone. In addition, DWI is a reasonable alternative to CE MRI in patients who cannot receive GBCAs.

1.2. Hepatocellular carcinoma (HCC)—HCC is the most common primary liver cancer and the third most common cause of cancer related death in the United States[83]. Early diagnosis is essential given improved prognosis of early stage HCC and advances in surgical and locoregional therapies (LRT)[84]. The diagnosis of HCC is made at CE-CT or CE-MRI for lesions > 1 cm that demonstrate arterial hyperenhancement and portal venous/late venous phase washout[5]. Of note, the sensitivity for detecting small HCC <2 cm is considerably lower using CE-CT or CE-MRI[85,86]. Several authors have investigated DWI as a tool to improve noninvasive HCC detection. DWI is moderately sensitive for the detection of HCC with detection rates ranging from 45–91.2%[71,87–89]. The wide range of reported sensitivities

likely reflects differences in study technique and selection bias, and thus, comparisons of reported results are somewhat challenging. Studies with very high reported sensitivities included either larger HCCs or cases with a high pre-test probability of HCC. Overall, DWI was better for HCC detection using low b value DWI (b0, b50) compared to conventional breath hold T2WI sequences (80.5% vs. 54%, $p < 0.001$) and especially for small HCCs < 2 cm (79% vs. 46%, $p<0.001$)[71]. Excellent detection rate of HCCs < 2 cm of 91.2% was shown in a series of 58 HCCs using high b value DWI compared to post-contrast and T2WI[88]. Overall, DWI has shown mixed results compared to CE-MRI. In the study by Piana et al, there was better sensitivity for HCC detection using DWI compared to CE T1WI in 91 patients with 109 HCCs greater than 1 cm in size (72.5–81.7% vs. 59.6–59.6%)[85]. In contrast, CE-MRI was superior for HCC detection in 52 patients with 72 HCCs in the only published liver explant DWI correlation study (87.9% vs. 75.8%, $p=0.02$)[90]. In another study, DWI and gadoxetic acid images showed equivalent pooled sensitivity for HCC detection (87.1% vs. 91.1%, $p > 0.05$) in 130 patients with 179 surgically confirmed HCCs in a separate series[91]. Fig. 4 demonstrates the classic imaging characteristics of HCC with DWI and CE-MRI. Finally, published data has shown that the combination of DWI, CE-MRI and/or HBP images yields the best sensitivity for HCC detection compared to either sequence alone[90,91]. Sensitivities as high as 97.9% may be achieved using this the combination of sequences[92]. The added benefit of the combination of sequences is that the DWI and CE MRI provide complimentary information: DWI is particularly useful in identifying lesions near vessels and CE MRI is useful for identifying subcapsular lesions or lesions in the left lobe. DWI may also be very helpful in detecting infiltrative HCC, which often does not demonstrate typical arterial hypervascularity and delayed wash-out appearance (Fig. 5)[93].

There are several possible explanations for the lower DWI detection rate for HCC. A recognized limitation of DWI sequences for HCC detection is that not all HCCs are hyperintense. Approximately 8.8–38.9% of HCC are either isointense or hypointense on DWI sequences, and smaller lesions (<2 cm) are frequently inconspicuous (Fig. 6) [85,94,95]. Well-differentiated HCC may be more frequently isointense than HCCs with higher tumor grade, however visual analysis of DW images alone is not reliable for this distinction[94,96]. The conspicuity and signal intensity of an HCC in a cirrhotic liver ultimately depend on a complex interaction between biologic and technical factors. HCCs are also more difficult to identify in the background of cirrhosis as the distorted liver parenchyma demonstrates diffusion restriction in relation with background fibrosis[97,98]. A retrospective study by Kim et al showed a trend towards decreased sensitivity for HCC detection with increasing severity of liver cirrhosis for two observers (Child-Pugh A 93.9–95.6%, Child-Pugh B 77.1–83.0%, Child-Pugh C 60.0–60.6%)[99]. Based on the data presented and the established benefits and limitations of each individual sequences, the optimal MRI protocol for detecting HCC in the cirrhotic liver should include the combination of DWI and CE/HBP MRI, thus yielding a maximized diagnostic accuracy.

Summary: DWI demonstrates moderate sensitivity for HCC detection. DWI should be used in combination with conventional MRI sequences, including post-contrast sequences, for HCC detection. Currently, DWI in isolation is insufficient for detecting HCC in cirrhosis.

1.3. Cholangiocarcinoma—Intrahepatic cholangiocarcinoma (ICC) is the second most common primary malignant tumor of the liver and is increasing in incidence[100]. Similar to HCC, ICC may arise in the context of hepatitis C and chronic liver disease[101]. There are three types of ICC classified based on morphology and growth pattern, including mass forming, periductal infiltrating type, and intraductal type[102]. The mass forming is the most common type and must be differentiated from HCC given the differences in treatment and prognosis. Recent reports have shown that small ICCs (< 3 cm) may have similar imaging appearance and enhancement pattern as HCC[103,104]. There is a paucity of data evaluating DWI imaging features and detection rates for ICC. Very few ICCs were included the previous work comparing DWI to T2 and CE-MRI. A recent study by Park et al describes a "target appearance" of ICC on DWI: peripheral hyperintense rim with a central area of hypointensity on high b-value images[105]. The central areas of hypointensity corresponded to fibrosis on histopathology. This finding was noted in 75% of ICCs (24/32) versus 3.1% of HCC (1/32) and may be a reliable imaging feature to distinguish small ICC from HCC. Further work is necessary to evaluate the role of DWI in the detection of ICC given its growing incidence and relatively poor prognosis.

Summary: There is limited data regarding the sensitivity of DWI for ICC detection. DWI may be of value in detecting ICC and shows a characteristic morphologic "target" appearance which should be verified in further studies.

2. Lesion characterization

2.1. Qualitative assessment—The noninvasive characterization of liver lesions without using GBCAs is increasingly attractive in the era of nephrogenic systemic fibrosis (NSF)[106]. Visual assessment of liver lesion morphology, signal intensity and changes in signal intensity at increasing b-values on DW images is useful for lesion characterization[6]. The changes in signal intensity observed on DW images over a range of b-values depend on true lesion water diffusivity, vascular microperfusion and T2 relaxation time. It is essential to separate true diffusion restriction from "T2 shine through". "T2 shine through" is the phenomenon present in lesions with long T2 relaxation times, such as cysts or gallbladder content, causing persistent hyperintensity on high b-value images and corresponding high ADC values; thus, the high signal observed is due to the long T2 of the lesion contents (fluid)[3]. The observed behavior of a lesion on qualitative images must therefore be interpreted along with the corresponding ADC map, which is the graphical representation of the ratio of the diffusion-weighted signal intensities[107]. Mean ADC values (mm^2/s) are obtained directly from the ADC map by placing a region of interest (ROI). ADC maps are calculated with a linear regression analysis of the function. The ROI used must be large enough to for sufficient SNR and to avoid the effects of volume averaging.

Previous work suggested that it is possible to characterize liver lesions as benign or malignant using DWI sequences[71,106,108–111]. Liver lesions are considered benign when demonstrating hyperintensity on low b-value DW images, attenuation of signal on higher b-value DWI images (b >500), and a corresponding high ADC value. Lesions are considered malignant when remaining hyperintense on higher b-value DW with a low corresponding ADC value[71,108] (Fig. 7). Performing visual assessment of lesion characterization has been shown to be highly accurate[71,108,112]. In a study of 185 focal liver lesions including 76

metastases and 11 HCCs, Holzapfel et al. demonstrated accuracy of 93% for characterizing small lesions <1 cm[113]. However, the majority of the benign lesions were cysts or hemangiomas. Of note, limitations of these reports include the relatively small sample sizes and limited types of liver lesions evaluated[106]. DWI may provide added benefit to conventional sequences in the characterization of indeterminate lesions in the cirrhotic liver. For example, distinguishing well-differentiated HCC from benign cirrhotic nodules remains challenging in many cases. In a recent study with histopathologic correlation, high b-value DWI showed higher accuracy (79%) than did hypointensity on HBP for distinguishing well-differentiated HCCs from benign cirrhotic nodules[114]. DWI was also useful in distinguishing hypervascular HCC from hypervascular pseudolesions, as no pseudolesions were hyperintense at DWI in a series by Motosugi et al[115]. In addition, indeterminate hypovascular lesions with diffusion restriction often go on to develop hypervascularity and overt imaging features of HCC; thus DWI may be a strong predictor for progression to hypervascular HCC[116].

Summary: Assessment of qualitative DW images allows for characterization of liver lesions as benign or malignant with a high degree of accuracy. DWI may play an added role to conventional sequences in characterizing indeterminate lesions in the cirrhotic liver.

2.2. Quantitative assessment—The ADC has been investigated as a tool to characterize liver lesions. As described previously in this text, the ADC is calculated from the diffusion sequence using multiple (at least 2) b-values. ADC quantification requires minimum acceptable SNR at higher b values and a minimum lesion size of 1.5–2 times the in-plane resolution in order to avoid partial volume averaging[6]. ADC images must be interpreted in conjunction with qualitative DW images and other sequences. Extensive prior work has shown that benign lesions generally have a significantly higher ADC value compared to malignant lesions[71,108,110,111,117–119]. Cysts and hemangiomas have statistically higher mean ADC values compared to all solid liver lesions (benign and malignant)[106]. In a large study of 542 lesions in 382 patients, the mean ADC values of specific liver lesions were as follows (measured as $\times 10^{-3}$ mm^2/s): cysts (3.40 ± 0.48), hemangiomas (2.26 ± 0.70), FNHs (1.79 ± 0.39), hepatocellular adenomas (1.49 ± 0.39), metastases (1.50 ± 0.65), and HCC (1.54 ± 0.44)[106]. ADC cutoff values between 1.4–1.6 × 10^{-3} mm^2/s have been reported in the literature for diagnosing malignant liver lesions, with reported sensitivities of 57.1–100% and specificities of 77–100% (Fig. 8) [71,106,108,110,118]. Of note, these ADC cutoff values vary depending on the patient population studied and DWI acquisition parameters. There is significant overlap in ADC measurement between solid benign and malignant lesions, thus making this distinction with DWI challenging. There is no statistically significant difference in reported ADC values for FNH, hepatocellular adenomas, metastases and HCC[106,120,121]. There is also a paucity of literature examining differences in ADC value for HCC, dysplastic (DN) and regenerative nodules (RN). A report by Xu et al did find that the ADC values of HCC were significantly lower than DN (1.28 × 10^{-3} mm^2/s vs. 1.53 × 10^{-3} mm^2/s, respectively, p=0.0082) in a series of 54 patients with 40 HCCs and 19 DNs, with histopathologic confirmation[122].

Summary: ADC quantification can be helpful in separating liver cysts and hemangiomas from malignant liver lesions. However, DWI with ADC quantification cannot reliably make the distinction between solid benign and malignant lesions, and between different malignant lesions.

2.3. Common pitfalls in using DWI for lesion characterization—There are several important limitations to DWI characterization of focal liver lesions. As stated, DWI and ADC characterization cannot distinguish between benign and malignant solid liver lesions given overlap in signal intensity and ADC values (Fig. 9). Furthermore, malignant lesions may be heterogeneous and may contain cystic, mucinous or necrotic components (Fig. 10). The T2 prolongation of these complex components results in elevated ADC values, allowing for mischaracterization of a malignant lesion as benign (Fig. 11)[3,6]. In addition, the ADC of liver abscesses can demonstrate significant overlap with both hemangiomas and solid lesions (Fig. 12)[106]. Thus, it is essential to rely on clinical history in addition to the imaging features on conventional sequences in order to correctly diagnose inhomogeneous metastasis and hepatic abscess.

Issues related to image quality may also affect interpretation of DWI and ADC. Patients with chronic liver disease and cirrhosis may have concomitant hepatic iron deposition, which may cause a significant T2 shortening effect in the liver that may result in decreased SNR on DW images, most pronounced on higher b values images, with falsely decreased ADC[123–125]. For example, ADC values were noted to be significantly lower in patients with hepatic siderosis in a series of 52 patients with cirrhosis[124]. Finally, interpretation of absolute ADC quantification has yet to be clarified as multiple factors influence ADC value (i.e. instrumental, sequencing, biologic). DW images are often of limited quality with relatively poor SNR, spatial resolution, and EPI related artifacts. DWI is still an imaging technique requiring image optimization to ensure consistent high quality performance[126].

Summary: Qualitative and quantitative information provided by DWI sequence is best used for characterizing cystic/necrotic lesions and highly cellular solid lesions. One must be aware of potential pitfalls and limitations when interpreting DW images and ADC maps.

3. Tumor treatment response

DWI has been investigated as a tool to evaluate tumor response to therapy and potentially predict which lesions will respond to treatment, by providing information regarding tumor viability, cellularity and vascularity[127]. Changes in DWI signal intensity and ADC following treatment can precede changes in lesion size or enhancement and reflect tumor necrosis[128]. The ability to detect early tumor treatment response or lack of response has significant impact in clinical management and treatment planning. Making this distinction would enable repeat treatment or alternative therapy if necessary. Furthermore, given the significant impact and adverse effects of current treatments, including chemotherapy and LRT, knowledge of how likely a lesion is to respond to therapy will also facilitate clinical decision-making in terms of how aggressively to pursue treatment[8].

Metastatic lesions to the liver have shown a significant increase in ADC values following systemic chemotherapy that precedes changes in lesion size[129,130]. Interestingly, a recent study by Marugami et al showed significant overlap in ADC values between responding and non-responding colorectal metastatic lesions following intra-arterial chemotherapy. Using a threshold change in ADC value of 3.5%, ROC analysis showed higher sensitivity and specificity values for % min ADC (100% and 92.6%, respectively) than for % mean ADC (66.7% and 74.1%, respectively) to identify responding lesions[131]. The % min ADC indicated the most diffusion restricting voxel within the ROI. Furthermore, liver metastases with low pre-treatment ADC values have responded better to systemic chemotherapy compared to lesions with high pre-treatment ADC values in several series. High pre-treatment ADC value of liver metastases is therefore a potential predictor of poor response to chemotherapy[8,129,132]. Metastatic lesions with higher ADC values may in fact have diminished blood supply and consequentially, more baseline cellular hypoxia and necrosis, which may limit the effectiveness of therapy. Another hypothesis to explain poor treatment response in lesions with high ADC value is the variation in local immune response: local host immune response results in increased tissue cellularity and cellular swelling, resulting in a lower ADC[8]. Fig. 13 demonstrates tumor recurrence in a patient with colon cancer who underwent wedge resection of the liver.

The development of LRT for HCC, including thermal radiofrequency ablation (RFA), trans-arterial chemoembolization (TACE), trans-arterial radioembolization (TARE), and external beam radiation, has revolutionized HCC treatment in non-operative patients or patients with unresectable disease. Lesions treated with RFA or TACE typically undergo coagulative hemorrhagic necrosis with heterogeneous hyperintensity on unenhanced T1WI, making evaluation of CE-MRI challenging[133]. Several authors have investigated DWI to evaluate HCC response to TACE and TARE[7,128,134–138]. LRT causes disruption of cellular membranes, cell death and tumor necrosis with the resultant increase in water diffusivity. An increase in ADC values has been reported following TACE in the early post-treatment period (few days up to 2 weeks) with measurable differences before and after treatment (Fig. 14)[7,128,135]. ADC values also increase post-TARE according to several preliminary series, but treatment effect has been noted at 1–3 months post-treatment [137,139,140]. ADC has demonstrated a significant correlation with tumor necrosis, especially complete tumor necrosis assessed with histopathology[141].

Furthermore, studies have demonstrated differences in ADC values between viable and necrotic portions of HCCs[7,141]. In theory, the viable portion of the tumor restricts diffusion (hyperintense with low ADC value), whereas the necrotic portions will show relatively un-impeded water diffusion (hyperintense with high ADC value)[142]. Fig. 15 demonstrates an example of a patient who underwent TACE and RFA to an index HCC with partial necrosis, in additional to additional tumors. Recent publications have also investigated the role of pre-treatment ADC value in predicting response to TACE, with discordant results. Mannelli et al showed that HCCs with low pre-TACE ADC tended to be less responsive to TACE than those with higher ADC, whereas Yuan et al showed that HCCs with higher pre-TACE ADC were less responsive than those with lower ADC to TACE[138,143]. Thus, DWI and ADC quantification may play a very important role in the non-invasive, non-contrast assessment of post-treatment response and guiding clinical treatment planning in a select population of

patients with HCC[144]. Pre-LRT ADC may be useful in predicting response to therapy; however large prospective studies are needed.

Summary: DWI is a potential useful non-invasive tool in evaluating response to therapy for liver metastases and HCC. Changes in ADC value precede changes in lesion size or enhancement, and correspond with tumor necrosis. Pre-treatment ADC values may also be of value in predicting response to treatment. Therefore, DWI and ADC quantification may provide early information valuable for treatment planning and clinical decision-making. However, large prospective studies are needed.

4. Liver fibrosis and cirrhosis

Liver fibrosis and cirrhosis affect parenchymal structure and function due to excessive extracellular matrix deposition. These microscopic changes may lead to reduced diffusion because of a larger proportion of macromolecules such as collagen (inducing restricted motion) and may also lead to reduced perfusion. Previous studies[16,17,98,145,146] have reported correlations between liver ADC and fibrosis stage assessed by histopathology. In most studies, a decrease in ADC was observed with increasing fibrosis stage and in cirrhosis. Lewin et al[145] reported AUCs of 0.79 and 0.92, for detection of stages F2–F4 and F3–F4, using ADC cutoff values of 1.24 and 1.21×10^{-3} mm^2/s, respectively. Taouli et al[98] observed AUCs of 0.896 and 0.896 for detection of stages F2–F4 and F3–F4, using cutoff values of 1.54 and 1.53×10^{-3} mm^2/s. Wang et al[146], in a study comparing DWI and MR elastography (MRE) for liver fibrosis detection, reported AUCs of 0.78–0.88 using ADC for detection of any stage of fibrosis, vs. AUC of 0.92–0.99 for MRE. Beyond ADC measurements, the IVIM technique has been tested recently for liver fibrosis and cirrhosis detection[14,16,17] with variable differences observed in fibrotic liver for both diffusion and perfusion metrics (Fig. 16). Fibrosis is, however not the only source of altered diffusion properties in the non-cirrhotic and cirrhotic liver. The influence of inflammatory response on ADC has been studied in lesions[147,148] and in the liver[26] showing restricted diffusion possibly because of increased viscosity. Increased fat content may also lead to reduced ADC[149].

LIMITATIONS

DWI sequence has several important limitations in terms of SS EPI image quality and ADC reproducibility. The SS EPI DWI sequence is limited given its relatively low spatial resolution and reduced SNR[6]. EPI artifacts including ghosting and distortion can result in image degradation, which is worse at higher field strength and in the left hepatic lobe. Despite gains in SNR, 3T SS EPI images may be further impaired by susceptibility artifacts caused by B1 inhomogeneities and dielectric/conductive artifacts[55,58]. Technical improvements including the application of strong gradients, multi-channel coils, high magnetic fields and advanced software platforms are being used to optimize DWI[6,126].

Significant variability in ADC values has been reported, likely as a result of a combination of hardware and biologic factors[6]. The CV of ADC values measured in liver parenchyma ranges from 3.0–16.2% in several reports[17,35,55,56]. Several authors have investigated ADC

reproducibility for malignant liver lesions. The DWI acquisition technique (BH, RT or FB), ADC calculation method, and selection of b-values all potentially influence the ADC measurement and the reproducibility for malignant liver lesions[150]. ADCs calculated from breath-hold DWI were more reproducible than from RT DWI in a recent study by Kim et al[150]. An additional recent study reports 95% limits of agreement of repeated ADC measurements of malignant liver lesions of 28.7–31.3% of the mean[36]. Greater reproducibility of ADC measurement for larger lesions and for lesions in the right hepatic lobe was also reported in this study[36], as well as in a recent study using IVIM[37]. Further improvements and modifications to the DWI sequence and ADC calculation are needed to optimize ADC measurement reproducibility and accuracy, thus enabling reliable comparison of research studies and evaluation post-treatment tumor response. Standardization of imaging technique and ADC calculation methods across imaging platforms may serve to address these issues.

Summary: DWI sequences are limited due to relative poor SNR and EPI related artifacts including ghosting and distortion. ADC quantification is limited by poor measurement reproducibility for both liver parenchyma and lesions. Future DWI sequence improvements and modifications are needed to address these limitations.

FUTURE DIRECTIONS

5.1. IVIM in the clinic

Emerging research has investigated the role of intravoxel incoherent motion (IVIM) for the following potential clinical applications:

5.1.1. Non-invasive detection of liver fibrosis—Given the experience with DWI and monoexponential ADC calculation, preliminary work has shown that IVIM can distinguish the individual contributions of cellular restricted diffusion and tissue perfusion, as defined by true diffusion coefficient (D), perfusion related pseudodiffusion (PF), and pseudodiffusion coefficient (D*)[16,17,35,151–153]. In a study comparing RT and FB IVIM using 9 b-values, there was a significant decrease in liver true diffusion coefficient (D), perfusion fraction (PF), pseudodiffusion coefficient (D*) and ADC in cirrhotic livers compared to healthy livers[17]. Similarly, a recent study using tri-exponential IVIM analysis also demonstrated a significant reduction in D*, D, and PF in cirrhosis[152]. In a prospective pilot study by Dyvorne et al evaluating the effect of diffusion gradient polarity and breathing acquisition on image quality, PF and D were reduced in patients with HCV related liver fibrosis[153]. Overall, these findings reflect the physiologic and microscopic cellular changes to the liver with fibrosis and cirrhosis: namely, the decrease in hepatic blood flow (reduction in portal flow) and the increased deposition of proteins and macromolecules (collagen). A current challenge in the role of IVIM for liver fibrosis quantification remains the optimization of image quality and standardization of the technique and inter-platform reproducibility, for which further research is necessary[44].

5.1.2. Liver lesion characterization—IVIM is being investigated for liver lesion characterization in hopes of addressing the existing challenges for ADC characterization, including the significant overlap in ADC values for benign and malignant lesions and the

variability in ADC measurement across imaging platforms. The ability to discriminate and measure diffusion and perfusion contributions may be of value for highly cellular and hypervascular lesions[151]. A recent study by Yoon et al retrospectively examined 142 patients with 169 focal liver lesions (120 malignant lesions), and found that the diagnostic performance of true diffusion (D) was better than that of ADC_{total} in the diagnosis of malignancy (AUC 0.971 using a cut off value 1.278×10^{-3} mm^2/s)[154]. In addition, the authors found that the perfusion fraction (PF) and pseudodiffusion coefficient (D*) were significantly higher in hypervascular lesions compared to hypovascular lesions. Microvascular flow in hypervascular lesions thus contaminated the ADC_{total} value, and therefore, the removal of perfusion contamination may be useful in revealing the increased cellularity in malignant hypervascular lesions thus allowing improved characterization[154]. The exciting new application of IVIM is limited by measurement reproducibility, for which further investigation is warranted[37,155].

5.2. Combination and comparison with PET/MRI

Recent technologic advancements have led to the integration of DWI with FDG-PET, a well-established functional modality for various oncologic and non-oncologic applications, allowing for simultaneous data acquisition. PET-MRI has the potential to combine excellent soft tissue contrast resolution, anatomic resolution and functional information with reduction in overall radiation exposure. DWI and PET are predicated upon entirely different fundamental principles and mechanisms, DWI assessing random motion of water and PET assessing cell glucose metabolism within biologic tissues. Maximum standardized uptake value (SUV_{max}) is a quantitative measure of cellular glucose metabolism and has been down shown to correlate with histopathologic tumor grade and the presence of necrosis[156,157]. These modalities can provide complementary information. DWI may be of value for lesions that are associated with low 18F-FDG accumulation and for the assessment of organs with normal high levels of background 18F-FDG accumulation. PET may be of value for lesions close to the heart or spleen[158].

Both DWI and PET can be acquired using FB technique with the ability to perform whole body imaging, multi-planar and 3-dimensional reformats. DWI and PET images are visually similar in appearance. Diagnostic performance of PET-MRI can be improved with acquisition of anatomic MR imaging sequences[159]. PET-MRI T1-weighted gradient-echo images and T2-weighted images have more accurate spatial registration than PET/CT images, although the DWI sequence can result in significant image misregistration from EPI-related geometric distortions, which is a potential weakness of the DWI-PET integration[160].

Studies on correlation between PET and DWI are limited, and results of preliminary work have shown an inverse relationship between ADC and SUV_{max}[161–163]. A recent prospective study was the first to examine correlation between SUV and ADC in neoplastic lesions using a simultaneous hybrid PET/MRI system. In this study, there was a significant negative correlation for between lesion SUV ratio (SUV_{max}/mean liver SUV) and ADC_{min} ($R=-0.46$, $p<0.04$) for non-osseous soft tissue lesions[164]. Well-designed prospective studies are needed to provide more insight and experience into the PET-DWI imaging integration, especially in

terms of patient tolerance, safety, diagnostic and prognostic capability and cost effectiveness[158]. Currently, there are no published clinical studies investigating the role of DWI-PET in liver malignancy.

5.3. New DWI sequences

The SS EPI sequence is the standard pulse sequence for liver MRI given its rapid acquisition time and relative insensitivity to patient motion[165]. Given enhancements in gradient systems and the emergence of parallel imaging, additional pulse sequences have been investigated for use in abdominal imaging, including spin-echo, stimulated-echo, fast-spin-echo, and steady-state free-precession sequences[166]. The most important alternative sequences used in the abdomen include the single-shot and PROPELLER fast-spin-echo and steady-state free-precession sequences[166]. Modifications of imaging parameters including selection of b-values is necessary when using these pulse sequence in order to obtain sufficient image quality and reliable quantification of diffusion parameters[166].

Diffusion tensor imaging (DTI), which employs additional sensitizing gradients to plot the relative degree of diffusion in multiple directions, has been studied in anatomy where diffusion is preferentially restricted in one direction[21]. DTI has been investigated in the central nervous system for evaluation of non-isotropic tissue such as white matter and spinal cord diseases. Limited data is available for DTI in the liver [25,52]. The use of multiple diffusion gradient directions with DTI results in a stronger applied gradient and shorter TE values[52]. Since more dimensions are plotted in DTI compared to conventional DWI, there is a theoretical advantage of more precise ADC calculation and information regarding tissue anisotropy. Preliminary work has investigated DTI in both healthy and fibrotic livers, with mixed results regarding image quality of DTI compared to conventional DWI[26]. Taouli et al showed no compromise in hepatic ADC values using DTI[52]. Further work is necessary to determine the role of DTI, if any, in the assessment of diffuse liver disease or focal liver lesion.

Summary: Emerging applications of DWI technology including IVIM, DWI/PET integration and new DWI sequences may further expand the role and ability of DWI to accurately detect and characterize diffuse and focal liver disease.

Conclusion

In this review, we have described our current understanding, applications and potential of DWI for the evaluation of focal and diffuse liver disease. DWI has many potential evolving applications, including focal liver lesion detection and characterization, the assessment of tumor response and the evaluation of diffuse liver disease. In our opinion, DWI should be incorporated into routine liver MRI protocols. DWI is best employed in combination with conventional sequences, especially contrast-enhanced sequences, for detection and characterization of malignant liver lesions. DWI currently has a limited role as an isolated technique for lesion characterization. The reader must be cognizant of the potential pitfalls and limitations of this technique. For patients with impaired renal function or GBCA allergy, DWI is a reasonable non-invasive alternative to CE MRI. Further sequence improvements and widespread standardization of technique, b-values and imaging parameters are necessary

for DWI to reach its full potential. Future applications including IVIM and DWI/PET MRI show promise and warrant further investigation.

References

1. Le Bihan D. Molecular diffusion nuclear magnetic resonance imaging. Magnetic resonance quarterly. Jan; 1991 7(1):1–30. [PubMed: 2043461]
2. Bammer R. Basic principles of diffusion-weighted imaging. European journal of radiology. Mar; 2003 45(3):169–184. [PubMed: 12595101]
3. Taouli B, Koh DM. Diffusion-weighted MR imaging of the liver. Radiology. Jan; 2010 254(1):47–66. [PubMed: 20032142]
4. Charnsangavej C, Clary B, Fong Y, Grothey A, Pawlik TM, Choti MA. Selection of patients for resection of hepatic colorectal metastases: expert consensus statement. Ann Surg Oncol. Oct; 2006 13(10):1261–1268. [PubMed: 16947009]
5. Bruix J, Sherman M, Llovet JM, et al. Clinical management of hepatocellular carcinoma. Conclusions of the Barcelona-2000 EASL conference. European Association for the Study of the Liver. Journal of hepatology. Sep; 2001 35(3):421–430. [PubMed: 11592607]
6. Galea N, Cantisani V, Taouli B. Liver lesion detection and characterization: Role of diffusion-weighted imaging. Journal of magnetic resonance imaging: JMRI. Jun; 2013 37(6):1260–1276. [PubMed: 23712841]
7. Kamel IR, Bluemke DA, Eng J, et al. The role of functional MR imaging in the assessment of tumor response after chemoembolization in patients with hepatocellular carcinoma. J Vasc Interv Radiol. Mar; 2006 17(3):505–512. [PubMed: 16567675]
8. Tam HH, Collins DJ, Brown G, et al. The role of pre-treatment diffusion-weighted MRI in predicting long-term outcome of colorectal liver metastasis. The British journal of radiology. Oct. 2013 86(1030):20130281. [PubMed: 23995873]
9. Holz M, Heil SR, Sacco A. Temperature-dependent self-diffusion coefficients of water and six selected molecular liquids for calibration in accurate 1H NMR PFG measurements. Physical Chemistry Chemical Physics. 2000; 2(20):4740–4742.
10. Stejskal EO, Tanner JE. Spin diffusion measurements: spin echoes in the presence of a time-dependent field gradient. J Chem Phys. 1965; 42:288–292.
11. Le Bihan D, Breton E, Lallemand D, Aubin ML, Vignaud J, Laval-Jeantet M. Separation of diffusion and perfusion in intravoxel incoherent motion MR imaging. Radiology. 1988; 168(2): 497–505. [PubMed: 3393671]
12. Koh DM, Collins DJ, Orton MR. Intravoxel incoherent motion in body diffusion-weighted MRI: reality and challenges. AJR Am J Roentgenol. Jun; 2011 196(6):1351–1361. [PubMed: 21606299]
13. Andreou A, Koh DM, Collins DJ, et al. Measurement reproducibility of perfusion fraction and pseudodiffusion coefficient derived by intravoxel incoherent motion diffusion-weighted MR imaging in normal liver and metastases. European radiology. Oct 6.2012
14. Dyvorne HA, Galea N, Nevers T, et al. Diffusion-weighted Imaging of the Liver with Multiple b Values: Effect of Diffusion Gradient Polarity and Breathing Acquisition on Image Quality and Intravoxel Incoherent Motion Parameters--A Pilot Study. Radiology. Dec 6.2012
15. Kang KM, Lee JM, Yoon JH, Kiefer B, Han JK, Choi BI. Intravoxel Incoherent Motion Diffusion-weighted MR Imaging for Characterization of Focal Pancreatic Lesions. Radiology. Oct 14.2013
16. Luciani A, Vignaud A, Cavet M, et al. Liver cirrhosis: intravoxel incoherent motion MR imaging--pilot study. Radiology. Dec; 2008 249(3):891–899. [PubMed: 19011186]
17. Patel J, Sigmund EE, Rusinek H, Oei M, Babb JS, Taouli B. Diagnosis of cirrhosis with intravoxel incoherent motion diffusion MRI and dynamic contrast-enhanced MRI alone and in combination: preliminary experience. Journal of magnetic resonance imaging: JMRI. Mar; 2010 31(3):589–600. [PubMed: 20187201]
18. Yamada I, Aung W, Himeno Y, Nakagawa T, Shibuya H. Diffusion coefficients in abdominal organs and hepatic lesions: evaluation with intravoxel incoherent motion echo-planar MR imaging. Radiology. Mar; 1999 210(3):617–623. [PubMed: 10207458]

19. Jensen JH, Helpern JA, Ramani A, Lu H, Kaczynski K. Diffusional kurtosis imaging: the quantification of non-gaussian water diffusion by means of magnetic resonance imaging. Magn Reson Med. Jun; 2005 53(6):1432–1440. [PubMed: 15906300]
20. Rosenkrantz AB, Sigmund EE, Winnick A, et al. Assessment of hepatocellular carcinoma using apparent diffusion coefficient and diffusion kurtosis indices: preliminary experience in fresh liver explants. Magnetic resonance imaging. Dec; 2012 30(10):1534–1540. [PubMed: 22819175]
21. Le Bihan D, Mangin JF, Poupon C, et al. Diffusion tensor imaging: concepts and applications. Journal of magnetic resonance imaging: JMRI. Apr; 2001 13(4):534–546. [PubMed: 11276097]
22. Gurses B, Kabakci N, Kovanlikaya A, et al. Diffusion tensor imaging of the normal prostate at 3 Tesla. European radiology. Apr; 2008 18(4):716–721. [PubMed: 17960389]
23. Kataoka M, Kido A, Yamamoto A, et al. Diffusion tensor imaging of kidneys with respiratory triggering: optimization of parameters to demonstrate anisotropic structures on fraction anisotropy maps. Journal of magnetic resonance imaging: JMRI. Mar; 2009 29(3):736–744. [PubMed: 19243070]
24. Manenti G, Carlani M, Mancino S, et al. Diffusion tensor magnetic resonance imaging of prostate cancer. Invest Radiol. Jun; 2007 42(6):412–419. [PubMed: 17507813]
25. Sigmund EE, Vivier PH, Sui D, et al. Intravoxel incoherent motion and diffusion-tensor imaging in renal tissue under hydration and furosemide flow challenges. Radiology. Jun; 2012 263(3):758–769. [PubMed: 22523327]
26. Taouli B, Chouli M, Martin AJ, Qayyum A, Coakley FV, Vilgrain V. Chronic hepatitis: role of diffusion-weighted imaging and diffusion tensor imaging for the diagnosis of liver fibrosis and inflammation. Journal of magnetic resonance imaging: JMRI. Jul; 2008 28(1):89–95. [PubMed: 18581382]
27. Cheung JS, Fan SJ, Gao DS, Chow AM, Man K, Wu EX. Diffusion tensor imaging of liver fibrosis in an experimental model. Journal of magnetic resonance imaging: JMRI. Nov; 2010 32(5):1141–1148. [PubMed: 21031520]
28. Taouli B, Vilgrain V, Dumont E, Daire JL, Fan B, Menu Y. Evaluation of liver diffusion isotropy and characterization of focal hepatic lesions with two single-shot echo-planar MR imaging sequences: prospective study in 66 patients. Radiology. Jan; 2003 226(1):71–78. [PubMed: 12511671]
29. Sasaki M, Yamada K, Watanabe Y, et al. Variability in absolute apparent diffusion coefficient values across different platforms may be substantial: a multivendor, multi-institutional comparison study. Radiology. Nov; 2008 249(2):624–630. [PubMed: 18936317]
30. Chenevert TL, Galban CJ, Ivancevic MK, et al. Diffusion coefficient measurement using a temperature-controlled fluid for quality control in multicenter studies. Journal of magnetic resonance imaging: JMRI. Oct; 2011 34(4):983–987. [PubMed: 21928310]
31. Girometti R, Furlan A, Esposito G, et al. Relevance of b-values in evaluating liver fibrosis: a study in healthy and cirrhotic subjects using two single-shot spin-echo echo-planar diffusion-weighted sequences. Journal of magnetic resonance imaging: JMRI. Aug; 2008 28(2):411–419. [PubMed: 18666139]
32. Xing D, Papadakis NG, Huang CL, Lee VM, Carpenter TA, Hall LD. Optimised diffusion-weighting for measurement of apparent diffusion coefficient (ADC) in human brain. Magnetic resonance imaging. 1997; 15(7):771–784. [PubMed: 9309608]
33. Lemke A, Stieltjes B, Schad LR, Laun FB. Toward an optimal distribution of b values for intravoxel incoherent motion imaging. Magnetic resonance imaging. Jul; 2011 29(6):766–776. [PubMed: 21549538]
34. Zhang JL, Sigmund EE, Rusinek H, et al. Optimization of b-value sampling for diffusion-weighted imaging of the kidney. Magn Reson Med. Jan; 2012 67(1):89–97. [PubMed: 21702062]
35. Braithwaite AC, Dale BM, Boll DT, Merkle EM. Short- and midterm reproducibility of apparent diffusion coefficient measurements at 3.0-T diffusion-weighted imaging of the abdomen. Radiology. Feb; 2009 250(2):459–465. [PubMed: 19095786]
36. Kim SY, Lee SS, Byun JH, et al. Malignant hepatic tumors: short-term reproducibility of apparent diffusion coefficients with breath-hold and respiratory-triggered diffusion-weighted MR imaging. Radiology. Jun; 2010 255(3):815–823. [PubMed: 20501719]

37. Kakite S, Dyvorne HA, Besa C, et al. Hepatocellular carcinoma: Short-term reproducibility of ADC and IVIM parameters at 3.0T. J Magn Reson Imag. (in press).
38. Le Bihan D, Poupon C, Amadon A, Lethimonnier F. Artifacts and pitfalls in diffusion MRI. Journal of magnetic resonance imaging: JMRI. Sep; 2006 24(3):478–488. [PubMed: 16897692]
39. Porter DA, Heidemann RM. High resolution diffusion-weighted imaging using readout-segmented echo-planar imaging, parallel imaging and a two-dimensional navigator-based reacquisition. Magn Reson Med. Aug; 2009 62(2):468–475. [PubMed: 19449372]
40. Lovblad KO, Jakob PM, Chen Q, et al. Turbo spin-echo diffusion-weighted MR of ischemic stroke. AJNR. American journal of neuroradiology. Feb; 1998 19(2):201–208. discussion 209. [PubMed: 9504466]
41. Lu L, Erokwu B, Lee G, et al. Diffusion-prepared fast imaging with steady-state free precession (DP-FISP): a rapid diffusion MRI technique at 7 T. Magn Reson Med. Sep; 2012 68(3):868–873. [PubMed: 22139974]
42. Deng J, Miller FH, Salem R, Omary RA, Larson AC. Multishot diffusion-weighted PROPELLER magnetic resonance imaging of the abdomen. Invest Radiol. Oct; 2006 41(10):769–775. [PubMed: 16971801]
43. Pipe JG. Motion correction with PROPELLER MRI: application to head motion and free-breathing cardiac imaging. Magn Reson Med. Nov; 1999 42(5):963–969. [PubMed: 10542356]
44. Kwee TC, Takahara T, Koh DM, Nievelstein RA, Luijten PR. Comparison and reproducibility of ADC measurements in breathhold, respiratory triggered, and free-breathing diffusion-weighted MR imaging of the liver. Journal of magnetic resonance imaging: JMRI. Nov; 2008 28(5):1141–1148. [PubMed: 18972355]
45. Taouli B, Sandberg A, Stemmer A, et al. Diffusion-weighted imaging of the liver: comparison of navigator triggered and breathhold acquisitions. Journal of magnetic resonance imaging: JMRI. Sep; 2009 30(3):561–568. [PubMed: 19711402]
46. Murtz P, Flacke S, Traber F, van den Brink JS, Gieseke J, Schild HH. Abdomen: diffusion-weighted MR imaging with pulse-triggered single-shot sequences. Radiology. Jul; 2002 224(1): 258–264. [PubMed: 12091693]
47. Johnson GA, Maki JH. In vivo measurement of proton diffusion in the presence of coherent motion. Invest Radiol. Jun; 1991 26(6):540–545. [PubMed: 1650333]
48. Ozaki M, Inoue Y, Miyati T, et al. Motion artifact reduction of diffusion-weighted MRI of the liver: use of velocity-compensated diffusion gradients combined with tetrahedral gradients. Journal of magnetic resonance imaging: JMRI. Jan; 2013 37(1):172–178. [PubMed: 22987784]
49. Griswold MA, Jakob PM, Heidemann RM, et al. Generalized autocalibrating partially parallel acquisitions (GRAPPA). Magn Reson Med. 2002; 47(6):1202–1210. [PubMed: 12111967]
50. Pruessmann KP, Weiger M, Scheidegger MB, Boesiger P. SENSE: sensitivity encoding for fast MRI. Magn Reson Med. Nov; 1999 42(5):952–962. [PubMed: 10542355]
51. Sodickson DK, Manning WJ. Simultaneous acquisition of spatial harmonics (SMASH): fast imaging with radiofrequency coil arrays. Magn Reson Med. Oct; 1997 38(4):591–603. [PubMed: 9324327]
52. Taouli B, Martin AJ, Qayyum A, et al. Parallel imaging and diffusion tensor imaging for diffusion-weighted MRI of the liver: preliminary experience in healthy volunteers. AJR Am J Roentgenol. Sep; 2004 183(3):677–680. [PubMed: 15333355]
53. Setsompop K, Gagoski BA, Polimeni JR, Witzel T, Wedeen VJ, Wald LL. Blipped-controlled aliasing in parallel imaging for simultaneous multislice echo planar imaging with reduced g-factor penalty. Magn Reson Med. May; 2012 67(5):1210–1224. [PubMed: 21858868]
54. Setsompop K, Cohen-Adad J, Gagoski BA, et al. Improving diffusion MRI using simultaneous multi-slice echo planar imaging. NeuroImage. Oct 15; 2012 63(1):569–580. [PubMed: 22732564]
55. Rosenkrantz AB, Oei M, Babb JS, Niver BE, Taouli B. Diffusion-weighted imaging of the abdomen at 3.0 Tesla: image quality and apparent diffusion coefficient reproducibility compared with 1.5 Tesla. Journal of magnetic resonance imaging: JMRI. Jan; 2011 33(1):128–135. [PubMed: 21182130]

56. Dale BM, Braithwaite AC, Boll DT, Merkle EM. Field strength and diffusion encoding technique affect the apparent diffusion coefficient measurements in diffusion-weighted imaging of the abdomen. Invest Radiol. Feb; 2010 45(2):104–108. [PubMed: 20027117]
57. Coenegrachts K, Delanote J, Ter Beek L, et al. Improved focal liver lesion detection: comparison of single-shot diffusion-weighted echoplanar and single-shot T2 weighted turbo spin echo techniques. The British journal of radiology. Jul; 2007 80(955):524–531. [PubMed: 17510250]
58. van den Bos IC, Hussain SM, Krestin GP, Wielopolski PA. Liver imaging at 3.0 T: diffusion-induced black-blood echo-planar imaging with large anatomic volumetric coverage as an alternative for specific absorption rate-intensive echo-train spin-echo sequences: feasibility study. Radiology. Jul; 2008 248(1):264–271. [PubMed: 18566178]
59. Okada Y, Ohtomo K, Kiryu S, Sasaki Y. Breath-hold T2-weighted MRI of hepatic tumors: value of echo planar imaging with diffusion-sensitizing gradient. Journal of computer assisted tomography. May-Jun;1998 22(3):364–371. [PubMed: 9606375]
60. Hussain SM, De Becker J, Hop WC, Dwarkasing S, Wielopolski PA. Can a single-shot black-blood T2-weighted spin-echo echo-planar imaging sequence with sensitivity encoding replace the respiratory-triggered turbo spin-echo sequence for the liver? An optimization and feasibility study. Journal of magnetic resonance imaging: JMRI. Mar; 2005 21(3):219–229. [PubMed: 15723376]
61. Moteki T, Horikoshi H. Evaluation of hepatic lesions and hepatic parenchyma using diffusion-weighted echo-planar MR with three values of gradient b-factor. Journal of magnetic resonance imaging: JMRI. Sep; 2006 24(3):637–645. [PubMed: 16888790]
62. Wu LM, Hu J, Gu HY, Hua J, Xu JR. Can diffusion-weighted magnetic resonance imaging (DW-MRI) alone be used as a reliable sequence for the preoperative detection and characterisation of hepatic metastases? A meta-analysis. Eur J Cancer. Feb; 2013 49(3):572–584. [PubMed: 23000072]
63. Cummings LC, Payes JD, Cooper GS. Survival after hepatic resection in metastatic colorectal cancer: a population-based study. Cancer. Feb 15; 2007 109(4):718–726. [PubMed: 17238180]
64. Benoist S, Nordlinger B. The role of preoperative chemotherapy in patients with resectable colorectal liver metastases. Ann Surg Oncol. Sep; 2009 16(9):2385–2390. [PubMed: 19554377]
65. Gillams AR, Lees WR. Five-year survival in 309 patients with colorectal liver metastases treated with radiofrequency ablation. European radiology. May; 2009 19(5):1206–1213. [PubMed: 19137310]
66. Koh DM, Collins DJ, Wallace T, Chau I, Riddell AM. Combining diffusion-weighted MRI with Gd-EOB-DTPA-enhanced MRI improves the detection of colorectal liver metastases. The British journal of radiology. Jul; 2012 85(1015):980–989. [PubMed: 22167501]
67. Zech CJ, Herrmann KA, Dietrich O, Horger W, Reiser MF, Schoenberg SO. Black-blood diffusion-weighted EPI acquisition of the liver with parallel imaging: comparison with a standard T2-weighted sequence for detection of focal liver lesions. Invest Radiol. Apr; 2008 43(4):261–266. [PubMed: 18340250]
68. Bruegel M, Gaa J, Waldt S, et al. Diagnosis of hepatic metastasis: comparison of respiration-triggered diffusion-weighted echo-planar MRI and five t2-weighted turbo spin-echo sequences. AJR Am J Roentgenol. Nov; 2008 191(5):1421–1429. [PubMed: 18941080]
69. d'Assignies G, Fina P, Bruno O, et al. High sensitivity of diffusion-weighted MR imaging for the detection of liver metastases from neuroendocrine tumors: comparison with T2-weighted and dynamic gadolinium-enhanced MR imaging. Radiology. Aug; 2013 268(2):390–399. [PubMed: 23533288]
70. Soyer P, Boudiaf M, Place V, et al. Preoperative detection of hepatic metastases: comparison of diffusion-weighted, T2-weighted fast spin echo and gadolinium-enhanced MR imaging using surgical and histopathologic findings as standard of reference. European journal of radiology. Nov; 2011 80(2):245–252. [PubMed: 20650588]
71. Parikh T, Drew SJ, Lee VS, et al. Focal liver lesion detection and characterization with diffusion-weighted MR imaging: comparison with standard breath-hold T2-weighted imaging. Radiology. Mar; 2008 246(3):812–822. [PubMed: 18223123]

72. Choi JS, Kim MJ, Choi JY, Park MS, Lim JS, Kim KW. Diffusion-weighted MR imaging of liver on 3.0-Tesla system: effect of intravenous administration of gadoxetic acid disodium. European radiology. May; 2010 20(5):1052–1060. [PubMed: 19915849]
73. Nasu K, Kuroki Y, Nawano S, et al. Hepatic Metastases: Diffusion-weighted Sensitivity-encoding versus SPIO-enhanced MR Imaging. Radiology. Apr; 2006 239(1):122–130. [PubMed: 16493012]
74. Koh DM, Brown G, Riddell AM, et al. Detection of colorectal hepatic metastases using MnDPDP MR imaging and diffusion-weighted imaging (DWI) alone and in combination. European radiology. May; 2008 18(5):903–910. [PubMed: 18193234]
75. Hardie AD, Naik M, Hecht EM, et al. Diagnosis of liver metastases: value of diffusion-weighted MRI compared with gadolinium-enhanced MRI. European radiology. Jun; 2010 20(6):1431–1441. [PubMed: 20148251]
76. Shimada K, Isoda H, Hirokawa Y, Arizono S, Shibata T, Togashi K. Comparison of gadolinium-EOB-DTPA-enhanced and diffusion-weighted liver MRI for detection of small hepatic metastases. European radiology. Nov; 2010 20(11):2690–2698. [PubMed: 20563726]
77. Chung WS, Kim MJ, Chung YE, et al. Comparison of gadoxetic acid-enhanced dynamic imaging and diffusion-weighted imaging for the preoperative evaluation of colorectal liver metastases. Journal of magnetic resonance imaging: JMRI. Aug; 2011 34(2):345–353. [PubMed: 21702068]
78. Holzapfel K, Reiser-Erkan C, Fingerle AA, et al. Comparison of diffusion-weighted MR imaging and multidetector-row CT in the detection of liver metastases in patients operated for pancreatic cancer. Abdominal imaging. Apr; 2011 36(2):179–184. [PubMed: 20563868]
79. Kenis C, Deckers F, De Foer B, Van Mieghem F, Van Laere S, Pouillon M. Diagnosis of liver metastases: can diffusion-weighted imaging (DWI) be used as a stand alone sequence? European journal of radiology. May; 2012 81(5):1016–1023. [PubMed: 21377305]
80. Lowenthal D, Zeile M, Lim WY, et al. Detection and characterisation of focal liver lesions in colorectal carcinoma patients: comparison of diffusion-weighted and Gd-EOB-DTPA enhanced MR imaging. European radiology. Apr; 2011 21(4):832–840. [PubMed: 20886339]
81. Kim YK, Lee MW, Lee WJ, et al. Diagnostic accuracy and sensitivity of diffusion-weighted and of gadoxetic acid-enhanced 3-T MR imaging alone or in combination in the detection of small liver metastasis (</= 1.5 cm in diameter). Invest Radiol. Mar; 2012 47(3):159–166. [PubMed: 22330426]
82. Macera A, Lario C, Petracchini M, et al. Staging of colorectal liver metastases after preoperative chemotherapy. Diffusion-weighted imaging in combination with Gd-EOB-DTPA MRI sequences increases sensitivity and diagnostic accuracy. European radiology. Mar; 2013 23(3):739–747. [PubMed: 22976920]
83. Parkin DM, Bray F, Ferlay J, Pisani P. Estimating the world cancer burden: Globocan 2000. International journal of cancer. Journal international du cancer. Oct 15; 2001 94(2):153–156. [PubMed: 11668491]
84. Bruix J, Llovet JM. Major achievements in hepatocellular carcinoma. Lancet. Feb 21; 2009 373(9664):614–616. [PubMed: 19231618]
85. Piana G, Trinquart L, Meskine N, Barrau V, Beers BV, Vilgrain V. New MR imaging criteria with a diffusion-weighted sequence for the diagnosis of hepatocellular carcinoma in chronic liver diseases. Journal of hepatology. Jul; 2011 55(1):126–132. [PubMed: 21145857]
86. Forner A, Vilana R, Ayuso C, et al. Diagnosis of hepatic nodules 20 mm or smaller in cirrhosis: Prospective validation of the noninvasive diagnostic criteria for hepatocellular carcinoma. Hepatology. Jan; 2008 47(1):97–104. [PubMed: 18069697]
87. Kim JE, Kim SH, Lee SJ, Rhim H. Hypervascular hepatocellular carcinoma 1 cm or smaller in patients with chronic liver disease: characterization with gadoxetic acid-enhanced MRI that includes diffusion-weighted imaging. AJR Am J Roentgenol. Jun; 2011 196(6):W758–765. [PubMed: 21606265]
88. Vandecaveye V, De Keyzer F, Verslype C, et al. Diffusion-weighted MRI provides additional value to conventional dynamic contrast-enhanced MRI for detection of hepatocellular carcinoma. European radiology. Oct; 2009 19(10):2456–2466. [PubMed: 19440718]

89. Hardie AD, Kizziah MK, Boulter DJ. Diagnostic accuracy of diffusion-weighted MRI for identifying hepatocellular carcinoma with liver explant correlation. Journal of medical imaging and radiation oncology. Aug; 2011 55(4):362–367. [PubMed: 21843170]

90. Park MS, Kim S, Patel J, et al. Hepatocellular carcinoma: detection with diffusion-weighted versus contrast-enhanced magnetic resonance imaging in pretransplant patients. Hepatology. Jul; 2012 56(1):140–148. [PubMed: 22370974]

91. Park MJ, Kim YK, Lee MW, et al. Small hepatocellular carcinomas: improved sensitivity by combining gadoxetic acid-enhanced and diffusion-weighted MR imaging patterns. Radiology. Sep; 2012 264(3):761–770. [PubMed: 22843769]

92. Xu PJ, Yan FH, Wang JH, Lin J, Ji Y. Added value of breathhold diffusion-weighted MRI in detection of small hepatocellular carcinoma lesions compared with dynamic contrast-enhanced MRI alone using receiver operating characteristic curve analysis. Journal of magnetic resonance imaging: JMRI. Feb; 2009 29(2):341–349. [PubMed: 19161186]

93. Rosenkrantz AB, Lee L, Matza BW, Kim S. Infiltrative hepatocellular carcinoma: comparison of MRI sequences for lesion conspicuity. Clinical radiology. Dec; 2012 67(12):e105–111. [PubMed: 23026725]

94. Nasu K, Kuroki Y, Tsukamoto T, Nakajima H, Mori K, Minami M. Diffusion-weighted imaging of surgically resected hepatocellular carcinoma: imaging characteristics and relationship among signal intensity, apparent diffusion coefficient, and histopathologic grade. AJR Am J Roentgenol. Aug; 2009 193(2):438–444. [PubMed: 19620441]

95. Kim YK, Kim CS, Han YM, Lee YH. Detection of liver malignancy with gadoxetic acid-enhanced MRI: is addition of diffusion-weighted MRI beneficial? Clinical radiology. Jun; 2011 66(6):489–496. [PubMed: 21367403]

96. Sandrasegaran K, Tahir B, Patel A, et al. The usefulness of diffusion-weighted imaging in the characterization of liver lesions in patients with cirrhosis. Clinical radiology. Jul; 2013 68(7):708–715. [PubMed: 23510619]

97. Sandrasegaran K, Akisik FM, Lin C, et al. Value of diffusion-weighted MRI for assessing liver fibrosis and cirrhosis. AJR Am J Roentgenol. Dec; 2009 193(6):1556–1560. [PubMed: 19933647]

98. Taouli B, Tolia AJ, Losada M, et al. Diffusion-weighted MRI for quantification of liver fibrosis: preliminary experience. AJR Am J Roentgenol. Oct; 2007 189(4):799–806. [PubMed: 17885048]

99. Kim AY, Kim YK, Lee MW, et al. Detection of hepatocellular carcinoma in gadoxetic acid-enhanced MRI and diffusion-weighted MRI with respect to the severity of liver cirrhosis. Acta Radiol. Oct 1; 2012 53(8):830–838. [PubMed: 22847903]

100. Patel T. Increasing incidence and mortality of primary intrahepatic cholangiocarcinoma in the United States. Hepatology. Jun; 2001 33(6):1353–1357. [PubMed: 11391522]

101. Kim SJ, Lee JM, Han JK, Kim KH, Lee JY, Choi BI. Peripheral mass-forming cholangiocarcinoma in cirrhotic liver. AJR Am J Roentgenol. Dec; 2007 189(6):1428–1434. [PubMed: 18029881]

102. Lim JH. Cholangiocarcinoma: morphologic classification according to growth pattern and imaging findings. AJR Am J Roentgenol. Sep; 2003 181(3):819–827. [PubMed: 12933488]

103. Vilana R, Forner A, Bianchi L, et al. Intrahepatic peripheral cholangiocarcinoma in cirrhosis patients may display a vascular pattern similar to hepatocellular carcinoma on contrast-enhanced ultrasound. Hepatology. Jun; 2010 51(6):2020–2029. [PubMed: 20512990]

104. Kim SA, Lee JM, Lee KB, et al. Intrahepatic mass-forming cholangiocarcinomas: enhancement patterns at multiphasic CT, with special emphasis on arterial enhancement pattern--correlation with clinicopathologic findings. Radiology. Jul; 2011 260(1):148–157. [PubMed: 21474703]

105. Park HJ, Kim YK, Park MJ, Lee WJ. Small intrahepatic mass-forming cholangiocarcinoma: target sign on diffusion-weighted imaging for differentiation from hepatocellular carcinoma. Abdominal imaging. Aug; 2013 38(4):793–801. [PubMed: 22829097]

106. Miller FH, Hammond N, Siddiqi AJ, et al. Utility of diffusion-weighted MRI in distinguishing benign and malignant hepatic lesions. Journal of magnetic resonance imaging: JMRI. Jul; 2010 32(1):138–147. [PubMed: 20578020]

107. Koh DM, Collins DJ. Diffusion-weighted MRI in the body: applications and challenges in oncology. AJR Am J Roentgenol. Jun; 2007 188(6):1622–1635. [PubMed: 17515386]

108. Mohr A, Priebe M, Taouli B, Grimm J, Heller M, Brossmann J. Selective water excitation for faster MR imaging of articular cartilage defects: initial clinical results. European radiology. Apr; 2003 13(4):686–689. [PubMed: 12664103]
109. Demir OI, Obuz F, Sagol O, Dicle O. Contribution of diffusion-weighted MRI to the differential diagnosis of hepatic masses. Diagn Interv Radiol. Jun; 2007 13(2):81–86. [PubMed: 17562512]
110. Ichikawa T, Haradome H, Hachiya J, Nitatori T, Araki T. Characterization of hepatic lesions by perfusion-weighted MR imaging with an echoplanar sequence. AJR Am J Roentgenol. Apr; 1998 170(4):1029–1034. [PubMed: 9530054]
111. Namimoto T, Yamashita Y, Sumi S, Tang Y, Takahashi M. Focal liver masses: characterization with diffusion-weighted echo-planar MR imaging. Radiology. Sep; 1997 204(3):739–744. [PubMed: 9280252]
112. Ichikawa T, Haradome H, Hachiya J, Nitatori T, Araki T. Diffusion-weighted MR imaging with a single-shot echoplanar sequence: detection and characterization of focal hepatic lesions. AJR Am J Roentgenol. Feb; 1998 170(2):397–402. [PubMed: 9456953]
113. Holzapfel K, Bruegel M, Eiber M, et al. Characterization of small (</=10 mm) focal liver lesions: value of respiratory-triggered echo-planar diffusion-weighted MR imaging. European journal of radiology. Oct; 2010 76(1):89–95. [PubMed: 19501995]
114. Lee MH, Kim SH, Park MJ, Park CK, Rhim H. Gadoxetic acid-enhanced hepatobiliary phase MRI and high-b-value diffusion-weighted imaging to distinguish well-differentiated hepatocellular carcinomas from benign nodules in patients with chronic liver disease. AJR Am J Roentgenol. Nov; 2011 197(5):W868–875. [PubMed: 22021534]
115. Motosugi U, Ichikawa T, Sou H, et al. Distinguishing hypervascular pseudolesions of the liver from hypervascular hepatocellular carcinomas with gadoxetic acid-enhanced MR imaging. Radiology. Jul; 2010 256(1):151–158. [PubMed: 20574092]
116. Kim YK, Lee WJ, Park MJ, Kim SH, Rhim H, Choi D. Hypovascular hypointense nodules on hepatobiliary phase gadoxetic acid-enhanced MR images in patients with cirrhosis: potential of DW imaging in predicting progression to hypervascular HCC. Radiology. Oct; 2012 265(1):104–114. [PubMed: 22891358]
117. Papanikolaou N, Gourtsoyianni S, Yarmenitis S, Maris T, Gourtsoyiannis N. Comparison between two-point and four-point methods for quantification of apparent diffusion coefficient of normal liver parenchyma and focal lesions. Value of normalization with spleen. European journal of radiology. Feb; 2010 73(2):305–309. [PubMed: 19091503]
118. Bruegel M, Holzapfel K, Gaa J, et al. Characterization of focal liver lesions by ADC measurements using a respiratory triggered diffusion-weighted single-shot echo-planar MR imaging technique. European radiology. Mar; 2008 18(3):477–485. [PubMed: 17960390]
119. Gourtsoyianni S, Papanikolaou N, Yarmenitis S, Maris T, Karantanas A, Gourtsoyiannis N. Respiratory gated diffusion-weighted imaging of the liver: value of apparent diffusion coefficient measurements in the differentiation between most commonly encountered benign and malignant focal liver lesions. European radiology. Mar; 2008 18(3):486–492. [PubMed: 17994317]
120. Sandrasegaran K, Akisik FM, Lin C, Tahir B, Rajan J, Aisen AM. The value of diffusion-weighted imaging in characterizing focal liver masses. Acad Radiol. Oct; 2009 16(10):1208–1214. [PubMed: 19608435]
121. Agnello F, Ronot M, Valla DC, Sinkus R, Van Beers BE, Vilgrain V. High-b-value diffusion-weighted MR imaging of benign hepatocellular lesions: quantitative and qualitative analysis. Radiology. Feb; 2012 262(2):511–519. [PubMed: 22143926]
122. Xu PJ, Yan FH, Wang JH, Shan Y, Ji Y, Chen CZ. Contribution of diffusion-weighted magnetic resonance imaging in the characterization of hepatocellular carcinomas and dysplastic nodules in cirrhotic liver. Journal of computer assisted tomography. Jul; 2010 34(4):506–512. [PubMed: 20657216]
123. Sener RN. Echo-planar and gradient-echo diffusion MRI of normal brain iron in the globus pallidus. Clinical imaging. Nov-Dec;2002 26(6):371–374. [PubMed: 12427429]
124. Chandarana H, Do RK, Mussi TC, et al. The effect of liver iron deposition on hepatic apparent diffusion coefficient values in cirrhosis. AJR Am J Roentgenol. Oct; 2012 199(4):803–808. [PubMed: 22997371]

125. Metwally MA, Zein CO, Zein NN. Clinical significance of hepatic iron deposition and serum iron values in patients with chronic hepatitis C infection. The American journal of gastroenterology. Feb; 2004 99(2):286–291. [PubMed: 15046219]
126. Chandarana H, Taouli B. Diffusion and perfusion imaging of the liver. European journal of radiology. Dec; 2010 76(3):348–358. [PubMed: 20399054]
127. Alonzi R, Hoskin P. Functional imaging in clinical oncology: magnetic resonance imaging- and computerised tomography-based techniques. Clin Oncol (R Coll Radiol). Sep; 2006 18(7):555–570. [PubMed: 16969988]
128. Kamel IR, Liapi E, Reyes DK, Zahurak M, Bluemke DA, Geschwind JF. Unresectable hepatocellular carcinoma: serial early vascular and cellular changes after transarterial chemoembolization as detected with MR imaging. Radiology. Feb; 2009 250(2):466–473. [PubMed: 19188315]
129. Cui Y, Zhang XP, Sun YS, Tang L, Shen L. Apparent diffusion coefficient: potential imaging biomarker for prediction and early detection of response to chemotherapy in hepatic metastases. Radiology. Sep; 2008 248(3):894–900. [PubMed: 18710982]
130. Anzidei M, Napoli A, Zaccagna F, et al. Liver metastases from colorectal cancer treated with conventional and antiangiogenetic chemotherapy: evaluation with liver computed tomography perfusion and magnetic resonance diffusion-weighted imaging. Journal of computer assisted tomography. Nov-Dec;2011 35(6):690–696. [PubMed: 22082538]
131. Marugami N, Tanaka T, Kitano S, et al. Early detection of therapeutic response to hepatic arterial infusion chemotherapy of liver metastases from colorectal cancer using diffusion-weighted MR imaging. Cardiovasc Intervent Radiol. Jul; 2009 32(4):638–646. [PubMed: 19238482]
132. Koh DM, Scurr E, Collins D, et al. Predicting response of colorectal hepatic metastasis: value of pretreatment apparent diffusion coefficients. AJR Am J Roentgenol. Apr; 2007 188(4):1001–1008. [PubMed: 17377036]
133. Kierans AS, Elazzazi M, Braga L, et al. Thermoablative treatments for malignant liver lesions: 10-year experience of MRI appearances of treatment response. AJR Am J Roentgenol. Feb; 2010 194(2):523–529. [PubMed: 20093619]
134. Kamel IR, Bluemke DA, Ramsey D, et al. Role of diffusion-weighted imaging in estimating tumor necrosis after chemoembolization of hepatocellular carcinoma. AJR Am J Roentgenol. Sep; 2003 181(3):708–710. [PubMed: 12933464]
135. Chen CY, Li CW, Kuo YT, et al. Early response of hepatocellular carcinoma to transcatheter arterial chemoembolization: choline levels and MR diffusion constants--initial experience. Radiology. May; 2006 239(2):448–456. [PubMed: 16569781]
136. Rhee TK, Omary RA, Gates V, et al. The effect of catheter-directed CT angiography on yttrium-90 radioembolization treatment of hepatocellular carcinoma. J Vasc Interv Radiol. Aug; 2005 16(8):1085–1091. [PubMed: 16105920]
137. Kamel IR, Reyes DK, Liapi E, Bluemke DA, Geschwind JF. Functional MR imaging assessment of tumor response after 90Y microsphere treatment in patients with unresectable hepatocellular carcinoma. J Vasc Interv Radiol. Jan; 2007 18(1 Pt 1):49–56. [PubMed: 17296704]
138. Mannelli L, Kim S, Hajdu CH, Babb JS, Taouli B. Serial diffusion-weighted MRI in patients with hepatocellular carcinoma: Prediction and assessment of response to transarterial chemoembolization. Preliminary experience. European journal of radiology. Apr; 2013 82(4): 577–582. [PubMed: 23246330]
139. Deng J, Miller FH, Rhee TK, et al. Diffusion-weighted MR imaging for determination of hepatocellular carcinoma response to yttrium-90 radioembolization. J Vasc Interv Radiol. Jul; 2006 17(7):1195–1200. [PubMed: 16868174]
140. Rhee TK, Naik NK, Deng J, et al. Tumor response after yttrium-90 radioembolization for hepatocellular carcinoma: comparison of diffusion-weighted functional MR imaging with anatomic MR imaging. J Vasc Interv Radiol. Aug; 2008 19(8):1180–1186. [PubMed: 18656011]
141. Mannelli L, Kim S, Hajdu CH, Babb JS, Clark TW, Taouli B. Assessment of tumor necrosis of hepatocellular carcinoma after chemoembolization: diffusion-weighted and contrast-enhanced MRI with histopathologic correlation of the explanted liver. AJR Am J Roentgenol. Oct; 2009 193(4):1044–1052. [PubMed: 19770328]

142. Lim KS. Diffusion-weighted MRI of hepatocellular carcinoma in cirrhosis. Clinical radiology. Sep 10.2013

143. Yuan Z, Ye XD, Dong S, et al. Role of magnetic resonance diffusion-weighted imaging in evaluating response after chemoembolization of hepatocellular carcinoma. European journal of radiology. Jul; 2010 75(1):e9–14. [PubMed: 19540083]

144. Yaghmai V, Besa C, Kim E, Gatlin JL, Siddiqui NA, Taouli B. Imaging assessment of hepatocellular carcinoma response to locoregional and systemic therapy. AJR Am J Roentgenol. Jul; 2013 201(1):80–96. [PubMed: 23789661]

145. Lewin M, Poujol-Robert A, Boelle PY, et al. Diffusion-weighted magnetic resonance imaging for the assessment of fibrosis in chronic hepatitis C. Hepatology. Sep; 2007 46(3):658–665. [PubMed: 17663420]

146. Wang Y, Ganger DR, Levitsky J, et al. Assessment of chronic hepatitis and fibrosis: comparison of MR elastography and diffusion-weighted imaging. AJR Am J Roentgenol. Mar; 2011 196(3): 553–561. [PubMed: 21343496]

147. Goyal A, Sharma R, Bhalla AS, Gamanagatti S, Seth A. Diffusion-weighted MRI in inflammatory renal lesions: all that glitters is not RCC! European radiology. Jan; 2013 23(1): 272–279. [PubMed: 22797980]

148. Kiryu S, Dodanuki K, Takao H, et al. Free-breathing diffusion-weighted imaging for the assessment of inflammatory activity in Crohn's disease. Journal of magnetic resonance imaging: JMRI. Apr; 2009 29(4):880–886. [PubMed: 19306416]

149. Poyraz AK, Onur MR, Kocakoc E, Ogur E. Diffusion-weighted MRI of fatty liver. Journal of magnetic resonance imaging: JMRI. May; 2012 35(5):1108–1111. [PubMed: 22170763]

150. Kim SY, Lee SS, Park B, et al. Reproducibility of measurement of apparent diffusion coefficients of malignant hepatic tumors: effect of DWI techniques and calculation methods. Journal of magnetic resonance imaging: JMRI. Nov; 2012 36(5):1131–1138. [PubMed: 22777895]

151. Le Bihan DBE, Lallemand D, Aubin ML, Vignaud J, Laval-Jeantet M. Separation of diffusion and perfusion in intravoxel incoherent motion MR imaging. Radiology. 1988; 168(2):497–505. [PubMed: 3393671]

152. Hayashi T, Miyati T, Takahashi J, et al. Diffusion analysis with triexponential function in liver cirrhosis. Journal of magnetic resonance imaging: JMRI. Jul; 2013 38(1):148–153. [PubMed: 23239543]

153. Dyvorne HA, Galea N, Nevers T, et al. Diffusion-weighted imaging of the liver with multiple b values: effect of diffusion gradient polarity and breathing acquisition on image quality and intravoxel incoherent motion parameters--a pilot study. Radiology. Mar; 2013 266(3):920–929. [PubMed: 23220895]

154. Yoon JH, Lee JM, Yu MH, Kiefer B, Han JK, Choi BI. Evaluation of hepatic focal lesions using diffusion-weighted MR imaging: Comparison of apparent diffusion coefficient and intravoxel incoherent motion-derived parameters. Journal of magnetic resonance imaging: JMRI. Apr 30.2013

155. Andreou A, Koh DM, Collins DJ, et al. Measurement reproducibility of perfusion fraction and pseudodiffusion coefficient derived by intravoxel incoherent motion diffusion-weighted MR imaging in normal liver and metastases. European radiology. Feb; 2013 23(2):428–434. [PubMed: 23052642]

156. Folpe AL, Lyles RH, Sprouse JT, Conrad EU 3rd, Eary JF. (F-18) fluorodeoxyglucose positron emission tomography as a predictor of pathologic grade and other prognostic variables in bone and soft tissue sarcoma. Clinical cancer research: an official journal of the American Association for Cancer Research. Apr; 2000 6(4):1279–1287. [PubMed: 10778952]

157. Rakheja R, Makis W, Skamene S, et al. Correlating metabolic activity on 18F-FDG PET/CT with histopathologic characteristics of osseous and soft-tissue sarcomas: a retrospective review of 136 patients. AJR Am J Roentgenol. Jun; 2012 198(6):1409–1416. [PubMed: 22623556]

158. Kwee TC, Takahara T, Ochiai R, et al. Complementary roles of whole-body diffusion-weighted MRI and 18F-FDG PET: the state of the art and potential applications. Journal of nuclear medicine: official publication, Society of Nuclear Medicine. Oct; 2010 51(10):1549–1558.

159. Tsushima Y, Takano A, Taketomi-Takahashi A, Endo K. Body diffusion-weighted MR imaging using high b-value for malignant tumor screening: usefulness and necessity of referring to T2-weighted images and creating fusion images. Acad Radiol. Jun; 2007 14(6):643–650. [PubMed: 17502253]

160. Rakheja R, Demello L, Chandarana H, et al. Comparison of the Accuracy of PET/CT and PET/MRI Spatial Registration of Multiple Metastatic Lesions. AJR Am J Roentgenol. Nov; 2013 201(5):1120–1123. [PubMed: 24147486]

161. Ho KC, Lin G, Wang JJ, Lai CH, Chang CJ, Yen TC. Correlation of apparent diffusion coefficients measured by 3T diffusion-weighted MRI and SUV from FDG PET/CT in primary cervical cancer. European journal of nuclear medicine and molecular imaging. Feb; 2009 36(2): 200–208. [PubMed: 18779960]

162. Wu X, Korkola P, Pertovaara H, Eskola H, Jarvenpaa R, Kellokumpu-Lehtinen PL. No correlation between glucose metabolism and apparent diffusion coefficient in diffuse large B-cell lymphoma: a PET/CT and DW-MRI study. European journal of radiology. Aug; 2011 79(2):e117–121. [PubMed: 21596501]

163. Gu J, Khong PL, Wang S, Chan Q, Law W, Zhang J. Quantitative assessment of diffusion-weighted MR imaging in patients with primary rectal cancer: correlation with FDG-PET/CT. Molecular imaging and biology: MIB: the official publication of the Academy of Molecular Imaging. Oct; 2011 13(5):1020–1028. [PubMed: 20872077]

164. Rakheja R, Chandarana H, Demello L, et al. Correlation Between Standardized Uptake Value and Apparent Diffusion Coefficient of Neoplastic Lesions Evaluated With Whole-Body Simultaneous Hybrid PET/MRI. AJR Am J Roentgenol. Nov; 2013 201(5):1115–1119. [PubMed: 24147485]

165. Turner R, Le Bihan D, Maier J, Vavrek R, Hedges LK, Pekar J. Echo-planar imaging of intravoxel incoherent motion. Radiology. Nov; 1990 177(2):407–414. [PubMed: 2217777]

166. Dietrich O, Biffar A, Baur-Melnyk A, Reiser MF. Technical aspects of MR diffusion imaging of the body. European journal of radiology. Dec; 2010 76(3):314–322. [PubMed: 20299172]

KEY POINTS

1. DWI (diffusion-weighted imaging) is based upon differences in mobility of water protons in tissues. Single-shot echo planar (SS EPI) DWI sequences are most commonly used in liver imaging.
2. DWI is generally more sensitive than fast spin echo fat suppressed T2-weighted imaging (T2WI) for liver lesion detection. The combination of DWI and CE-T1 weighted imaging (contrast-enhanced T1-WI) is most sensitive for detection of malignant liver lesions.
3. ADC (apparent diffusion coefficient) quantification can be used to characterize liver lesions as cystic/necrotic or solid. However, ADC alone is insufficient for lesion characterization.
4. ADC has potential value in the evaluation of tumor treatment response, with changes in ADC preceding changes in lesion size.
5. ADC quantification and IVIM (intra voxel incoherent motion) DWI have diagnostic value in the non-invasive detection of liver fibrosis and cirrhosis.

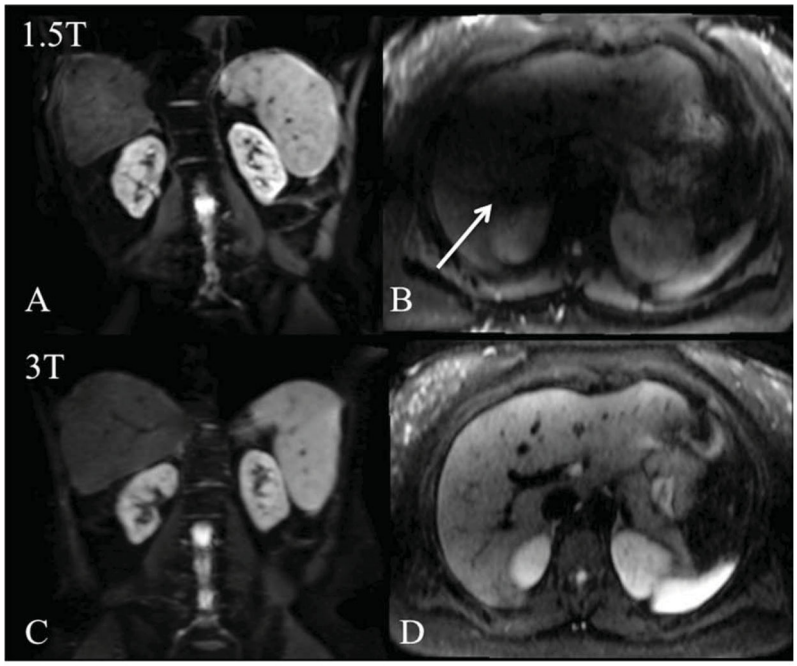

Fig. 1.

Example of increased SS EPI diffusion artifacts at 3T (A–B) compared to 1.5T (C–D) in the same patients imaged with both systems (b400 images are shown). Image distortion on coronal SS EPI image due to higher B0 inhomogeneity (A) is observed in a 62 y male patient with HCV and fibrosis. Signal drop due to B1 field inhomogeneity at 3T (arrow on B) is observed in a 24 y female healthy subject, compared to 1.5T (D).

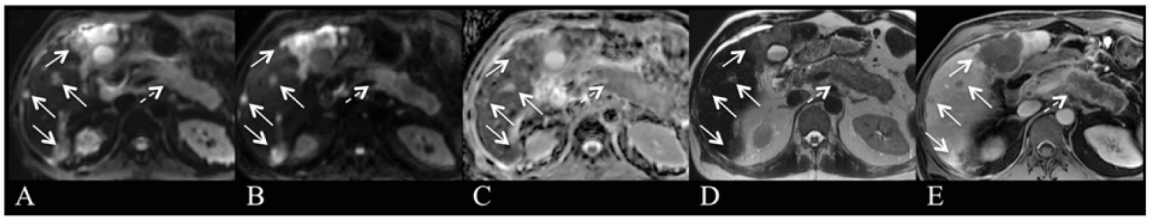

Fig. 2.

51-year-old male with pancreatic cancer and liver metastases. Axial RT SS EPI DWI at 3T with b values of 50 and 800 s/mm^2 (A, B) and ADC map (C), FSE T2WI (E) and axial late venous phase GRE T1-WI after injection of extracellular contrast medium (E). Both liver metastases (arrows) and the primary pancreatic tumor with secondary pancreatic duct distention (dashed arrow) are identified on b50 images (A), and remain hyperintense on high b value image (B). ADC value of the largest confluent metastasis was 0.97×10^{-3} mm^2/s.

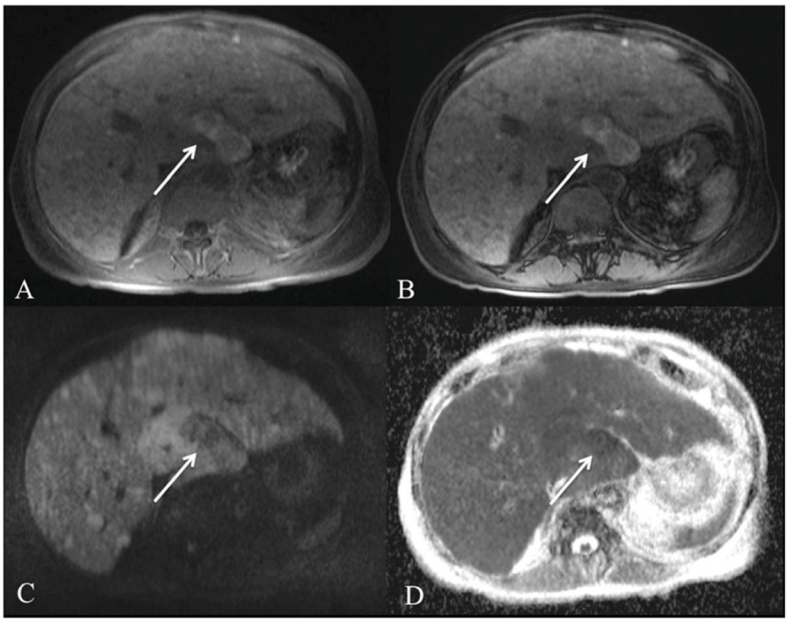

Fig. 3.

80 year old male with diffuse metastatic melanoma. Axial T1 in-phase (A) and opposed phase images (B), axial RT SS EPI DWI with b value of 1000 s/mm^2 (C) and ADC map (D). Innumerable non-fat containing T1 hyperintense lesions are present throughout the liver, the largest confluent lesion measuring 5.2 cm in the caudate lobe (arrow). Lesions demonstrate diffusion restriction with low signal on ADC map (ADC value 0.87×10^{-3} mm^2/s).

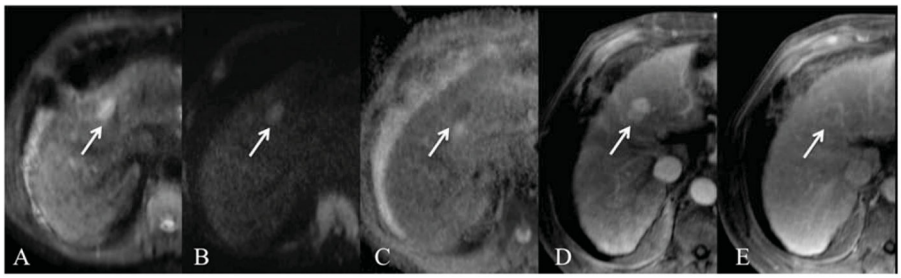

Fig. 4.

66-year-old male with HCC. Axial RT SS EPI DWI at 1.5T with b values of 50 and 1000 s/mm^2 (A,B) and ADC map (C), contrast-enhanced (using extracellular contrast medium) T1WI on arterial phase (D) and late venous phase (E). There is a left hepatic lobe HCC (arrow) which is hyperintense on b50 (A) and b1000 (B) images with low ADC (1.31×10^{-3} mm^2/s). The lesion demonstrates typical hypervascular hyperenhancement (D) with delayed phase washout and pseudocapsular enhancement (E).

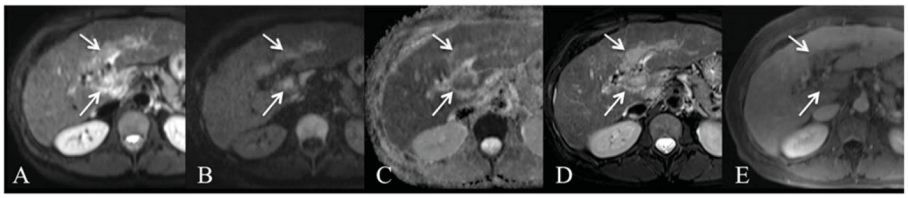

Fig. 5.

59-year-old female with infiltrative HCC invading the portal vein. Axial free breathing SS EPI DWI with b values of 50 and 1000 s/mm^2 (A, B) and ADC map (C), fat suppressed FSE T2WI (D) and contrast-enhanced (using extracellular contrast medium) T1WI at portal venous phase (E). Tumor thrombus (arrows) demonstrates T2 hyperintensity and restricted diffusion on both b50 (A) and b1000 (B) images with low corresponding ADC value 1.45 × 10^{-3} mm^2/s. The extent of tumor is better delineated on the DWI and T2 images (arrows, A–D) compared to post-contrast image (E).

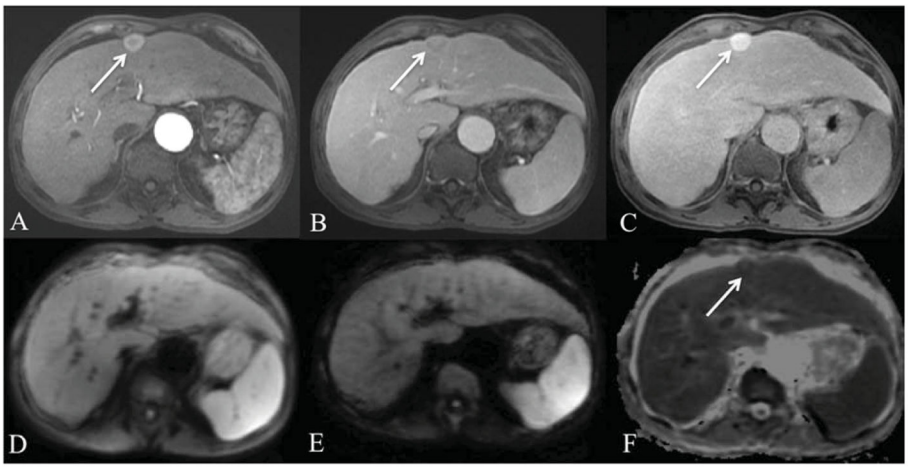

Fig. 6.

63-year-old male with hepatitis C cirrhosis and HCC. Axial arterial phase (A), portal venous phase (B), delayed hepatobiliary phase (C), axial free breathing SS EPI DWI with b values of 50 (D) and 500 s/mm^2 (E) and ADC map (F) after injection of gadoxetic acid. 2.4 cm left hepatic lobe lesion (arrow) is hypervascular with portal venous phase washout/delayed pseudocapsule enhancement and demonstrates hyperintensity on delayed hepatobiliary phase images. The lesion is isointense on both low and high b-value DWI images and ADC map, with ADC value of 1.49×10^{-3} mm^2/s. A well-differentiated HCC was found at histopathology.

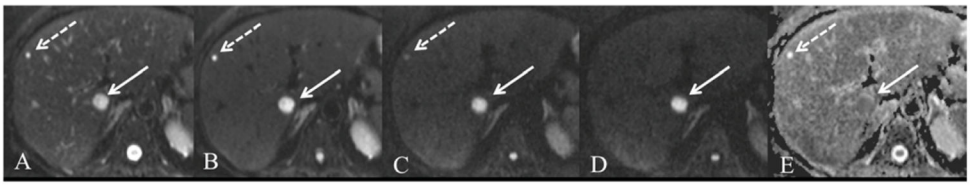

Fig. 7.

58 year old female with metastatic colon cancer and hepatic cyst. Axial respiratory-triggered SS EPI DWI at 1.5T with b values of 0, 50, 500 and 800 s/mm^2 (A–D) and ADC map (E). Both lesions are easily detected on b50 images (B) with excellent suppression of intrahepatic vascular flow. The liver metastasis (solid arrow) remains hyperintense on high b value with low ADC (1.1×10^{-3} mm^2/s). The cyst (dashed arrow) shows strong signal drop on intermediate b-value images and is not seen on high b value with high ADC (3.2×10^{-3} mm^2/s).

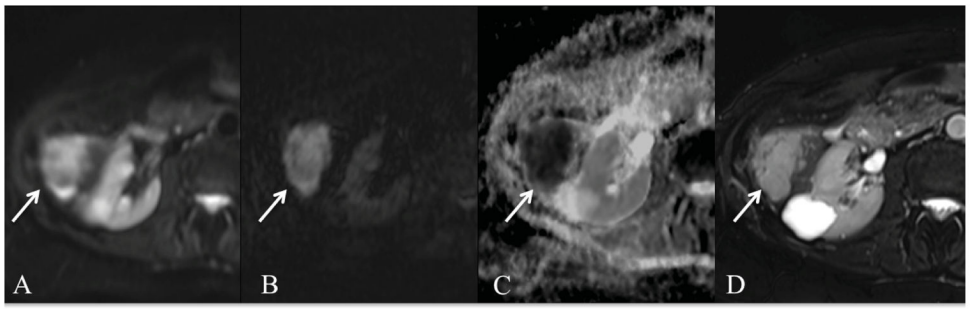

Fig. 8.

79-year-old female with subcapsular ovarian cancer metastasis. Axial respiratory triggered SS EPI DWI at 1.5T with b values of 50 and 1000 s/mm2 (A, B) and ADC map (C), and fat suppressed FSE T2WI (D). There is a metastatic lesion that is T2 hyperintense with diffusion restriction. ADC value was 1.0×10^{-3} mm^2/s.

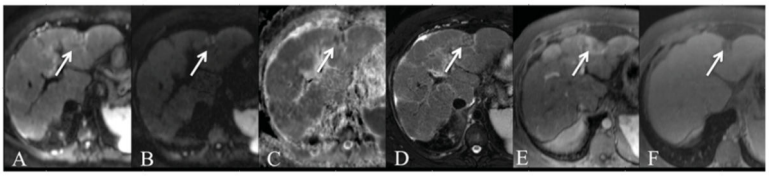

Fig. 9.

29-year-old male with biopsy-proven necrotizing granuloma. Axial RT SS EPI DWI with b values of 50 and 1000 s/mm^2 (A, B) and ADC map (C), fat suppressed FSE T2WI (D) and gadobutrol enhanced GRE T1WI on arterial and equilibrium phases (E, F). There is a T2-weighted hypointense, enhancing lesion in segment 2 with foci of restricted diffusion and adjacent capsular retraction (arrow). ADC value was 1.19×10^{-3} mm^2/s.

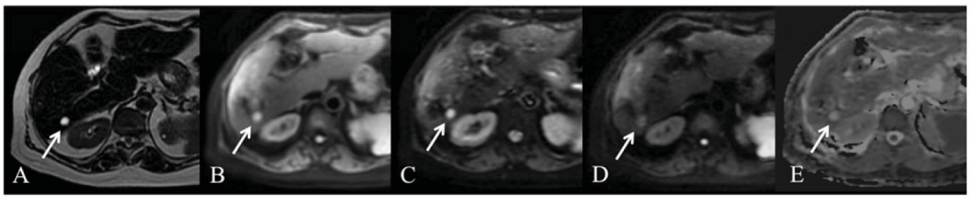

Fig. 10.

61 year old female with cystic metastasis (arrow). Axial T2 SSFSE (A), breath hold axial SS EPI DWI with b 50, 100, 500 (B, C, D) and ADC map (E). There is a 1.2 cm cystic lesion in segment 6 which is markedly hyperintense on T2 SSFSE. The lesion is hyperintense on low b value image with attenuation of signal on high b value images and high ADC signal (ADC value 3.4×10^{-3} mm^2/s) (arrow). Imaging characteristics are consistent with a benign cyst, however this lesion represented a cystic neuroendocrine metastasis.

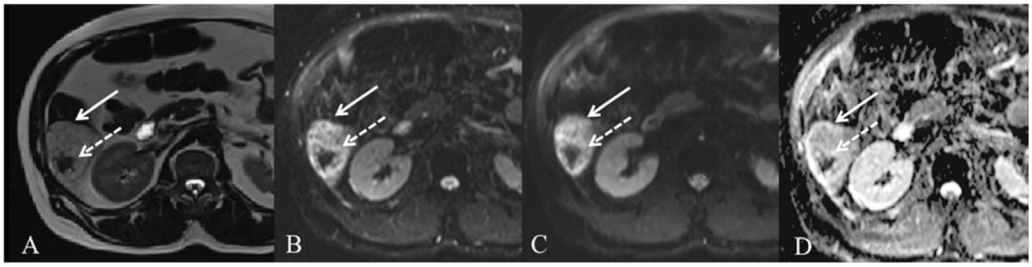

Fig. 11.

57 year old male with indeterminate liver lesion. There is a 6.9 cm segment 6 lesion (arrow) which is hyperintense on axial HASTE (A), FB SS EPI DWI b50 (B) and b500 (C) with corresponding high signal on ADC map (D). ADC value measured as 1.6×10^{-3} mm^2/s. The central hypointense area represents susceptibility artifact from intra-lesional hemorrhage (dashed arrow) with corresponding "T2 black out" on DWI images. Given atypical findings on post-contrast T1WI (not shown), lesion was considered indeterminate and biopsy revealed epitheloid angiosarcoma.

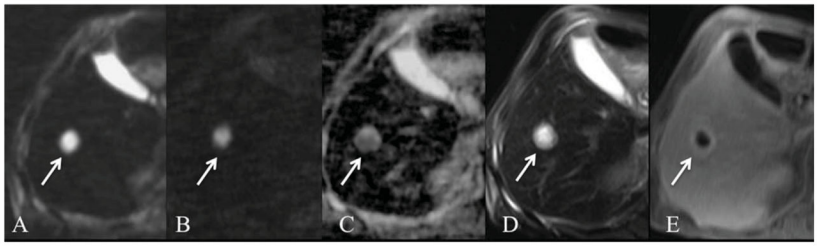

Fig. 12.

67-year-old male status post chemotherapy for diffuse large B-cell lymphoma. Axial respiratory triggered SS EPI DWI with b values of 50 and 800 s/mm^2 (A, B) and ADC map (C), fat suppressed FSE T2WI (D) and gadobutrol enhanced GRE T1WI on late venous phase (E). A thick-walled T2 hyperintense lesion is present in the right hepatic lobe (arrow) demonstrating peripheral rim enhancement (E) and centrally restricted diffusion on both b 50 (A) and b750 (B). FNA guided biopsy of the lesion revealed pus, compatible with hepatic abscess.

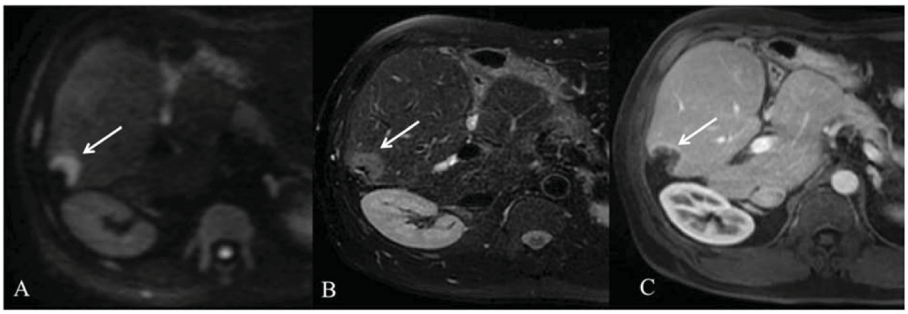

Fig. 13.

51 year old male status post partial right wedge resection for metastatic colon cancer with tumor recurrence. Axial respiratory-triggered SS EPI DWI with b value of 500 s/mm2 (A), axial breath-hold fat suppressed T2WI (B), and axial fat-suppressed GRE T1WI after gadoxetic acid injection at portal venous phase (C) show a hypovascular metastatic lesion at the resection margin (arrow), which is hyperintense on DWI and T2WI.

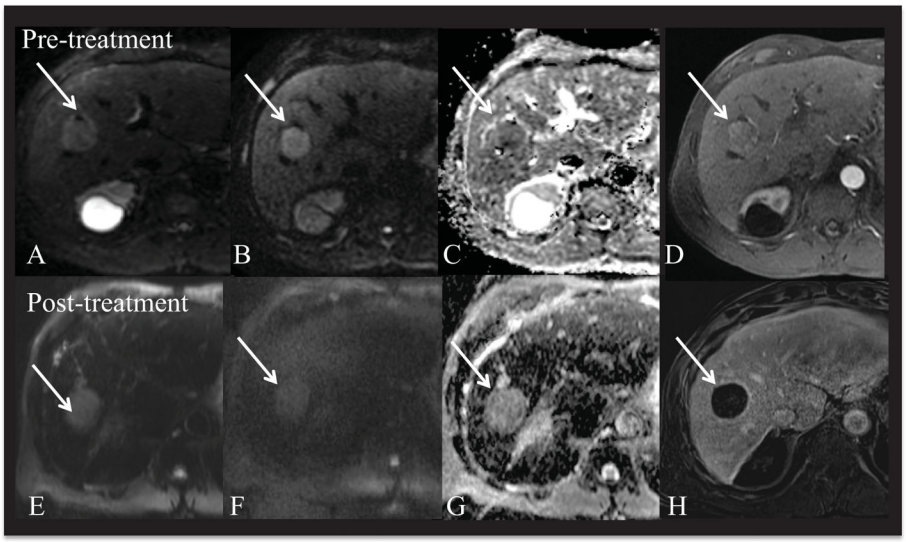

Fig. 14.

66 year old male with hepatitis C related cirrhosis and HCC. 3.2 cm HCC in segment 8 (arrow). Pre-treatment MRI (top) and post-treatment MRI (bottom row). Respiratory-triggered SS EPI DWI at b50, 1000 (A, B) and ADC (C) and arterial phase CE T1WI (gadobutrol) (D) demonstrate HCC in the right lobe with restricted diffusion (ADC value of 1.0×10^{-3} mm^2/s). Patient underwent right hepatic lobe Y-90 radio-embolization. Follow-up MRI using free breathing SS EPI DWI at b50, b1000 (E, F) and ADC (G) demonstrate a significant increase in ADC value of 1.7×10^{-3} mm^2/s. Post-contrast subtracted (H) image demonstrates complete interval necrosis.

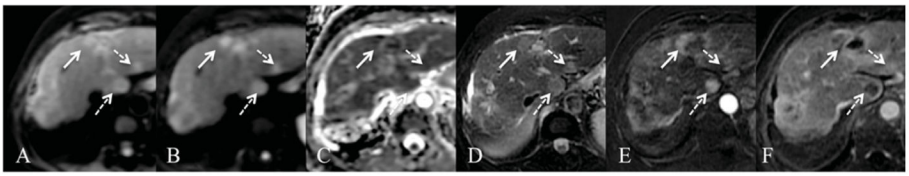

Fig. 15.

79-year-old female status post TACE/RFA of left hepatic lobe HCC. Axial free breathing SS EPI DWI with b values of 50 and 500 s/mm^2 (A,B) and ADC map (C), fat suppressed FSE T2WI (D) and gadoxetate enhanced GRE T1WI on arterial phase (E) and late phase subtraction images (F). A left lobe approximately 50% necrotic treated HCC and adjacent arterial enhancing nodule (E) with venous wash-out (F) are present (arrow). The viable nodule shows T2-weighted hyperintensity (D) and restricted diffusion (A, B) with low ADC value of 0.70×10^{-3} mm^2/s. There are additional HCCs in the left and caudate lobes (dashed arrows).

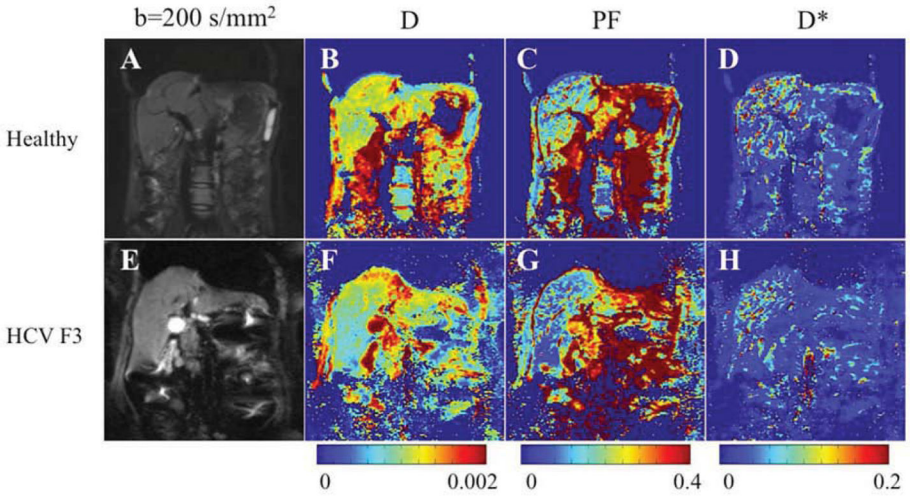

Fig. 16.

Parametric IVIM diffusion maps obtained with respiratory-triggered SS EPI sequence and 16 b-values (0–800) in a 26-year-old healthy woman and a 55-year-old woman with HCV and stage F3 fibrosis. A, E, Coronal single-shot echo-planar image DW image (b200). B, F: true diffusion coefficient (D) map. C, G: perfusion fraction (PF) map. D, H, D* (pseudodiffusion coefficient) map. D and PF maps show lower values in patient with HCV than in healthy subject. There is no visible difference in D* maps. Corresponding parameter values were: for D, 0.81 10^{-3} mm^2/s and 1.06 10^{-3} mm^2/s for the patient with HCV and the healthy volunteer, respectively; for PF, 5.1% and 9.8%, respectively; and for D*, 50.5 × 10^{-5} mm^2/s and 49.4 × 10^{-5} mm^2/s, respectively.

From: Dyvorne HA, Galea N, Nevers T, et al. Diffusion-weighted imaging of the liver with multiple b values: effect of diffusion gradient polarity and breathing acquisition on image quality and intravoxel incoherent motion parameters--a pilot study. Radiology 2013;266: 920–929; with permission.